JOURNAL OF PETROLOGY | VOLUME 44 | NUMBER 3 | PAGES 569–602 | 2003

Petrogenesis of Basanitic to Tholeiitic Volcanic Rocks from the Miocene Vogelsberg, Central Germany

P. J. F. BOGAARD* AND G. WÖRNER†

GEOWISSENSCHAFTLICHES ZENTRUM GÖTTINGEN, GEORG AUGUST UNIVERSITÄT GÖTTINGEN, GOLDSCHMIDTSTRASSE 1, 37077 GÖTTINGEN, GERMANY

RECEIVED JUNE 21, 2001; ACCEPTED JULY 25, 2002

The Miocene Vogelsberg volcano in Central Germany produced mafic magmas ranging in composition from basanite to quartz tholeiite and limited amounts of evolved magmas. Trace element and Nd, Sr and Pb isotopic compositions reveal the presence of three distinct mantle sources: (1) a trace element enriched, asthenospheric plume-type source, similar to the European Asthenospheric Reservoir composition inferred for many other Tertiary volcanic provinces in Central Europe; (2) a depleted mantle source, located in the lithospheric mantle or uppermost asthenosphere; (3) a veined lithospheric mantle source. The oldest basanites of the Vogelsberg volcano have distinctly higher Ti, Al, Sc and V contents than younger basanites. These high-Ti basanites may have been produced by partial melting of a veined lithospheric mantle source, formed during the earliest stages of uplift of the Rhenish Shield, ~70 Myr ago. Younger basanites were generated by small degrees of partial melting of the European Asthenospheric Reservoir, whereas alkali basalts and tholeiites formed by mixing of variable proportions of melts derived from the European Asthenospheric Reservoir and depleted mantle sources, respectively. These magmas then interacted with metasomatized sub-continental lithospheric mantle, which explains the observed range in Sr, Nd and Pb isotopic compositions. Subsequently the most depleted tholeiites were contaminated by lower-crustal rocks. The distinct stratigraphic position of the various lava groups in the 656·5 m 'Forschungsbohrung Vogelsberg 1996' borehole and the correlation of their chemical stratigraphy with palaeomagnetic reversals reflects an episodic temporal evolution of magmas and mantle sources. During Stage I, melts from the veined lithospheric mantle source were pooled in crustal magma chambers and evolved to erupt a range of differentiated lavas. In Stage II melts were formed in the depleted mantle source and up-section gradually mixed with melts from the asthenospheric mantle. In Stage III the depleted mantle source was exhausted and pure asthenospheric melts were erupted.

KEY WORDS: *crustal contamination; mantle sources; Sr, Nd and Pb isotopes; temporal evolution of magmas and sources; trace elements; Vogelsberg*

INTRODUCTION

Primitive mafic volcanic rocks from different regions within the Tertiary Central European Volcanic Province (CEVP) define distinct geochemical trends on Sr–Nd–Pb isotope diagrams that converge on a common source composition (Wilson & Downes, 1991; Cebriá & Wilson, 1995; Hoernle *et al*., 1995). These isotope signatures reflect the involvement of a common, plume-related, asthenospheric component known as the Low Velocity Component (LVC; Hoernle *et al*., 1995) or European Asthenospheric Reservoir (EAR; Cebriá & Wilson, 1995), and regionally differing sub-continental lithospheric mantle (SCLM) components (Cebriá & Wilson, 1995; Granet *et al*., 1995; Hoernle *et al*., 1995). The composition and origin of these mantle components has been deduced from trace element and isotopic compositions of erupted lavas spanning a wide range of ages and geographical locations. Although models have been

*Present address: Faculty of Earth and Life Sciences, Vrije Universiteit Amsterdam, De Boelelaan 1085, 1081 HV Amsterdam, The Netherlands.

†Corresponding author. Telephone: +49-(0)551-393971. Fax: +49-(0)551-393982. E-mail: gwoerne@gwdg.de

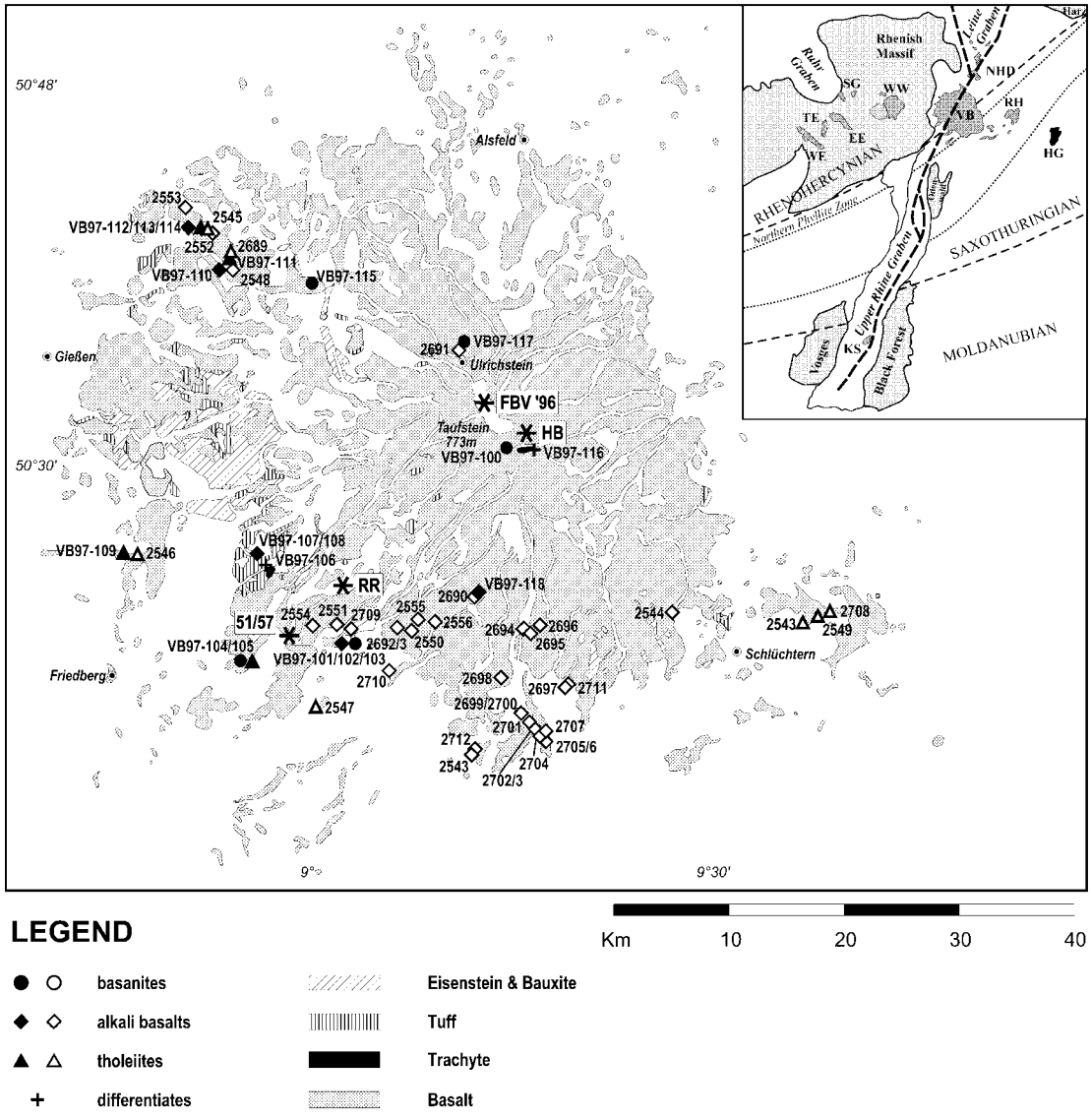

Fig. 1. Map showing currently exposed volcanic rocks of the Vogelsberg. Drill-core locations are shown by stars [FBV: Forschungsbohrung Vogelsberg 1996, samples VB96-01 to VB96-92; HB: Hasselborn 2/2a (Ehrenberg *et al*., 1981), samples VB98-130 to VB98-137; RR: Rainrod 1 (Ernst *et al*., 1970), samples VB98-138 to VB98-145; 51/57: Drill cores 51 and 57, camptonites 11175, 11309 and 11315]. Filled symbols show field sample locations from this study; open symbols are for samples from Wittenbecher (1992). The inset shows Tertiary–Quaternary volcanic fields and major structural units of Central Germany (after Schreiber & Rotsch, 1998). WE, West Eifel; TE, Tertiary Eifel; EE, East Eifel; SG, Siebengebirge; WW, Westerwald; VB, Vogelsberg; NHD, Northern Hessian Depression; RH, Rhön; HG, Heldburger Gangschar; KS, Kaiserstuhl.

developed (e.g. Granet *et al*., 1995), thus far the temporal evolution and physical distribution of the mantle components with respect to the location and development of the melting region below a single Central European volcanic edifice has never been conclusively documented.

The Miocene Vogelsberg volcano (Fig. 1) erupted basanites and alkali basalts, (quartz) tholeiites, and limited amounts of highly evolved magmas ranging from hawaiite to trachyte. Here we evaluate the petrogenesis of the various volcanic rock types of the Vogelsberg based on detailed sampling of a new 656·5 m drill core in the central Vogelsberg (Forschungsbohrung Vogelsberg 1996 or FBV; Fig. 2), samples from the Hasselborn 2/2a and Rainrod I drill cores (Ernst *et al*., 1970; Kreuzer *et al*., 1974; Ehrenberg *et al*., 1981) and field locations (Fig. 1). The sampling of drill cores allows us to evaluate the mantle sources of Vogelsberg magmatism within the context of its temporal evolution. We identify three distinct mantle

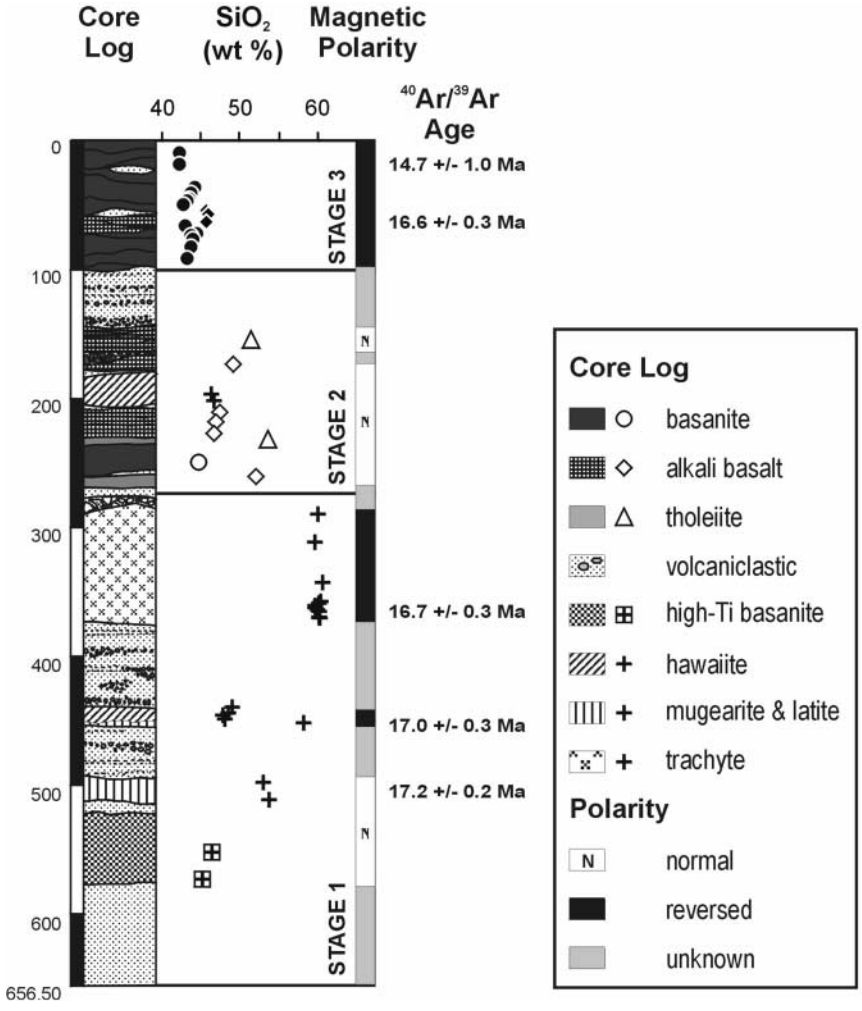

Fig. 2. Core log of the FBV. SiO_2 contents of fresh basalt flows demonstrate that abrupt changes in chemistry, correlated with reversals in magnetic polarity [see Schnepp *et al.* (2001) for palaeomagnetic data], define three magmatic stages. Details on $^{40}Ar/^{39}Ar$ ages are given in an Electronic Appendix, available from the *Journal of Petrology* website at http://www.petrology.oupjournals.org, and by Bogaard (2000).

sources: (1) an enriched component with trace element and isotopic signatures similar to those of the EAR, which is asthenospheric in origin and probably related to the upwelling of anomalously hot mantle material; (2) a depleted component derived from the uppermost asthenosphere or lowermost lithospheric mantle; (3) a source component with a trace element and isotopic composition similar, but not identical, to that of the EAR, which contains a large proportion of hydrous minerals.

The clear stratigraphic control on the various geochemical signatures of samples from the FBV drill core, Ar–Ar age dating (Bogaard, 2000) and field sampling allows the establishment of an evolutionary model for the Vogelsberg volcano and its mantle source region through time.

GEOLOGY AND VOLCANIC STRATIGRAPHY

With an eruptive volume of $\sim 600\,km^3$, the Miocene Vogelsberg volcano is one of the largest volcanic centres of the CEVP. It is a broadly circular shield volcano with a diameter of ~ 50 km and a maximum thickness estimated at ~ 800 m (Ehrenberg & Hickethier, 1985). The volcano is situated directly to the east of the Rhenish Massif, close to the triple junction of the Rhine, Ruhr and Leine Grabens (Fig. 1). The Vogelsberg straddles the Northern Phyllite zone of the Variscan orogen of central Europe.

The asthenosphere–lithosphere boundary below the SE part of the Rhenish Massif is elevated to ~ 60 km depth (Babuska & Plomerova, 1992) and lies at

$\sim$70 km depth below the Vogelsberg (Braun & Berckhemer, 1993). The lower crust is characterized by a strongly reflective zone at $\sim$20 km depth, and a transition zone from crustal to mantle velocities between 20 and 28 km depth (Raikes & Bonjer, 1983; Braun & Berckhemer, 1993). This zone may indicate massive intrusion of basic magma at the crust–mantle boundary (Raikes & Bonjer, 1983).

Volcanism in the Vogelsberg commenced in the Aquitanian (Ehrenberg *et al.*, 1981), but the main phase of volcanic activity began $\sim$18 Myr ago and peaked between 16 and 17 Ma (Bogaard, 2000, and references therein). The Vogelsberg drill core shows that volcanic rocks were erupted in three stages that differ both in chemistry and eruptive character (Fig. 2). The first and oldest stage, Stage I, is largely confined to the central part of the Vogelsberg and comprises a large range of compositions from basanites to hawaiites, mugearites, latites and trachytes (Fig. 3). The basanites of this stage have distinctly higher TiO_2, Al_2O_3 and Zr/Nb, and lower MgO (Figs 3 and 4) than the basanites of Stage III (see below), and are here referred to as high-Ti basanites. The earliest lava flows of the first stage erupted $\sim$18 Myr ago (Ehrenberg *et al.*, 1981). A thick trachyte flow represents the final product and was dated at 16·7 $\pm$ 0·3 Ma (Bogaard, 2000).

Stage II comprises alkali basalts and tholeiites. Tholeiites are most abundant in the outer reaches of the Vogelsberg. They have high SiO_2 contents (52–56 wt %), and their low MgO (5·6–7·9 wt %), Ni (71–166 ppm) and Cr (132–344 ppm) contents provide clear evidence of fractional crystallization. Alkali basalts span a range in compositions from 46 to 52 wt % SiO_2 and are compositionally intermediate between primitive basanites and evolved tholeiites (see Fig. 3). None of these rocks contained suitable material for Ar–Ar age dating.

The third stage (III) comprises basanites and primitive alkali basalts (<46 wt % SiO_2). Their primitive character is evidenced by high Mg-numbers (67–74), Ni (225–473 ppm) and Cr (336–633 ppm), as well as the common presence of mantle xenoliths. Two flows of this stage, one near the middle and the other at the top, were dated at 16·6 $\pm$ 0·3 Ma and 14·7 $\pm$ 1·0 Ma, respectively (Bogaard, 2000).

The three stages correlate with magnetic polarity reversals, suggesting that each stage was formed in a short active period that in turn was followed by a magmatic quiet period. The stages represent eruption of different magma batches, each characterized by (1) different magma sources and (2) different styles of magmatic evolution (Bogaard *et al.*, 2001*b*).

In addition to the above, several camptonites were analysed. These occur in dykes that cut the Palaeozoic–Mesozoic basement of the Vogelsberg (Ehrenberg & Hickethier, 1978). The samples analysed here are derived from drill cores in the southern Vogelsberg. Samples 11175 and 11309 were dated at 67·8 $\pm$ 0·1 and 68·9 $\pm$ 0·4 Ma, respectively (Bogaard, 2000). The camptonites therefore are not part of the Vogelsberg volcanism, but their major and trace element characteristics show some striking similarities (high TiO_2 and low MgO contents, similar Zr/Nb ratios; Figs 3 and 4) to high-Ti basanites and may therefore provide important clues to the origin of the high-Ti basanites.

The Rhön and Northern Hessian Depression volcanic fields are closely related in space and time to the Vogelsberg and produced basanites, alkali basalts and tholeiites with similar characteristics to the Vogelsberg rocks (Wedepohl, 1985; Ehrenberg & Hickethier, 1994; Wedepohl *et al.*, 1994; Jung & Hoernes, 2000). High-Ti basanites do not occur in the Northern Hessian Depression, but hornblende basalts with high amphibole contents are found as early volcanic products both in the Rhön (Ehrenberg & Hickethier, 1994) and in drill cores in the southern Vogelsberg (Ehrenberg & Hickethier, 1978). Although these rocks are petrographically different from high-Ti basanites from the FBV, Hasselborn 2/2a and Rainrod I drill cores, they do have high TiO_2 and low MgO concentrations, and similar Zr/Nb (Jung & Hoernes, 2000).

ANALYTICAL METHODS

Major and minor oxides and the trace elements Sc, V, Cr, Co, Ni, Zn, Ga, Rb, Sr, Y, Zr, Nb and Ba were analysed by X-ray fluorescence (XRF) using a Philips-PW 1408 XRF spectrometer. Analyses were carried out on lithium borate glass fusion beads. Relative precision (2σ) was generally better than 2% for the major oxides and better than 10% for trace elements. The remaining trace elements were analysed by inductively coupled plasma mass spectrometry (ICP-MS) on a VG-PlasmaQuad STE ICP mass spectrometer. The samples were dissolved in a Teflon pressure bomb, using a 1:1 mixture of HF and $HClO_4$ at 180°C, and then taken up in an HNO_3 solution with an In–Re internal standard. Because the high field strength elements (HFSE) have a strong tendency to hydrolyse and polymerize in solution (Hall & Plant, 1992; Totland *et al.*, 1992), selected samples were reanalysed for HFSE using a modified procedure (Muenker, 1998). After dissolution in HF–$HClO_4$, the samples were taken up in a mixture of HNO_3, 6N HCl and HF and diluted. These solutions were measured within 24 h after dilution, to prevent absorption of HFSE on the sample bottle. Together with the sample solutions, special calibration solutions were prepared for the

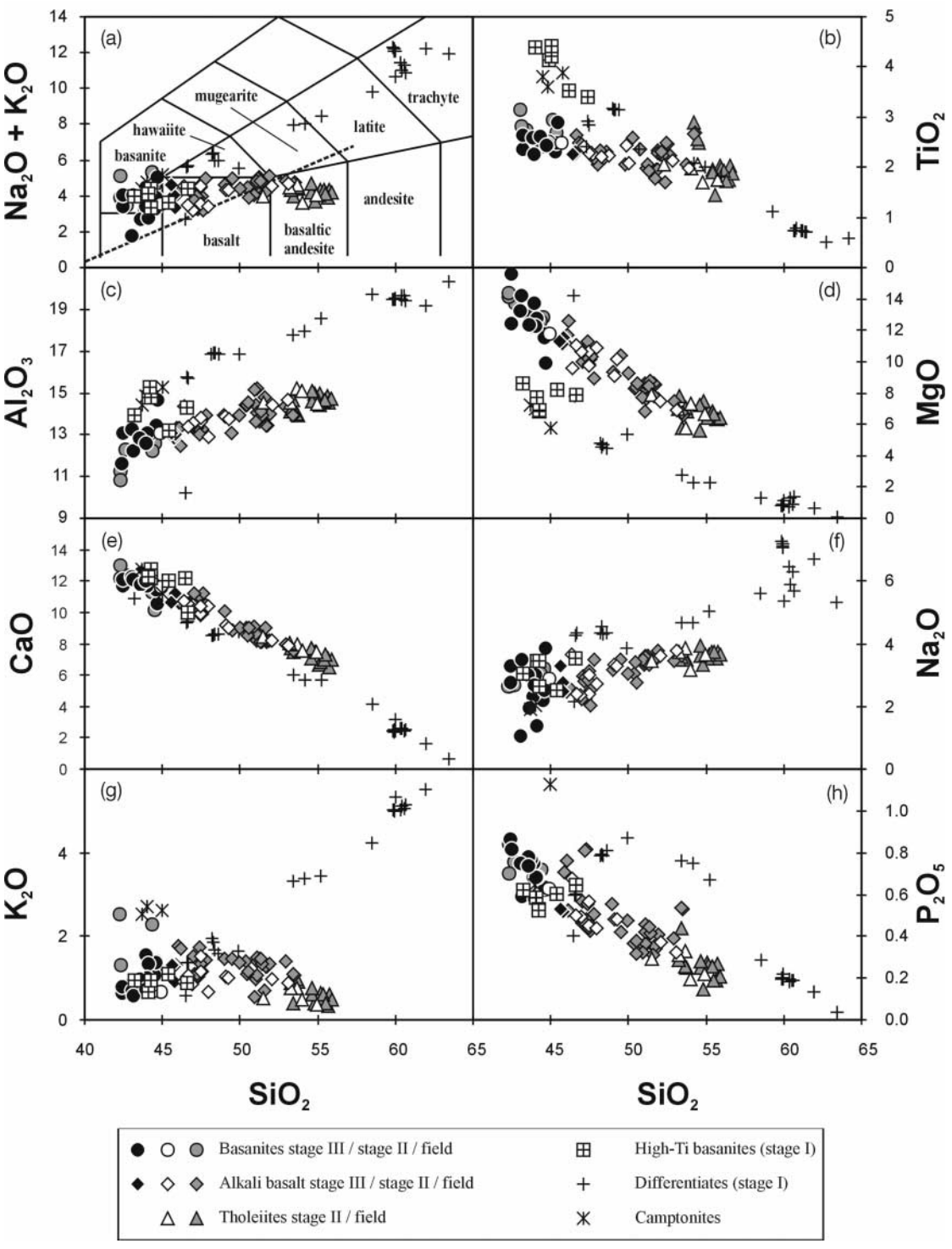

Fig. 3. Major element variation for Vogelsberg volcanic rocks. Colour coding of samples corresponds to their stratigraphic position; +, Stage I; open symbols, Stage II; filled symbols, Stage III. Grey symbols indicate field samples that cannot be assigned unequivocally to a specific stage. Camptonites (stars) are veins recovered from drill cores below the base of the Vogelsberg volcanic sequence. These rocks are much older than the Vogelsberg volcanism (dated at 67·8 ± 0·1 and 68·9 ± 0·4 Ma; Bogaard, 2000), but have major and trace element characteristics very similar to those of Vogelsberg high-Ti basanites.

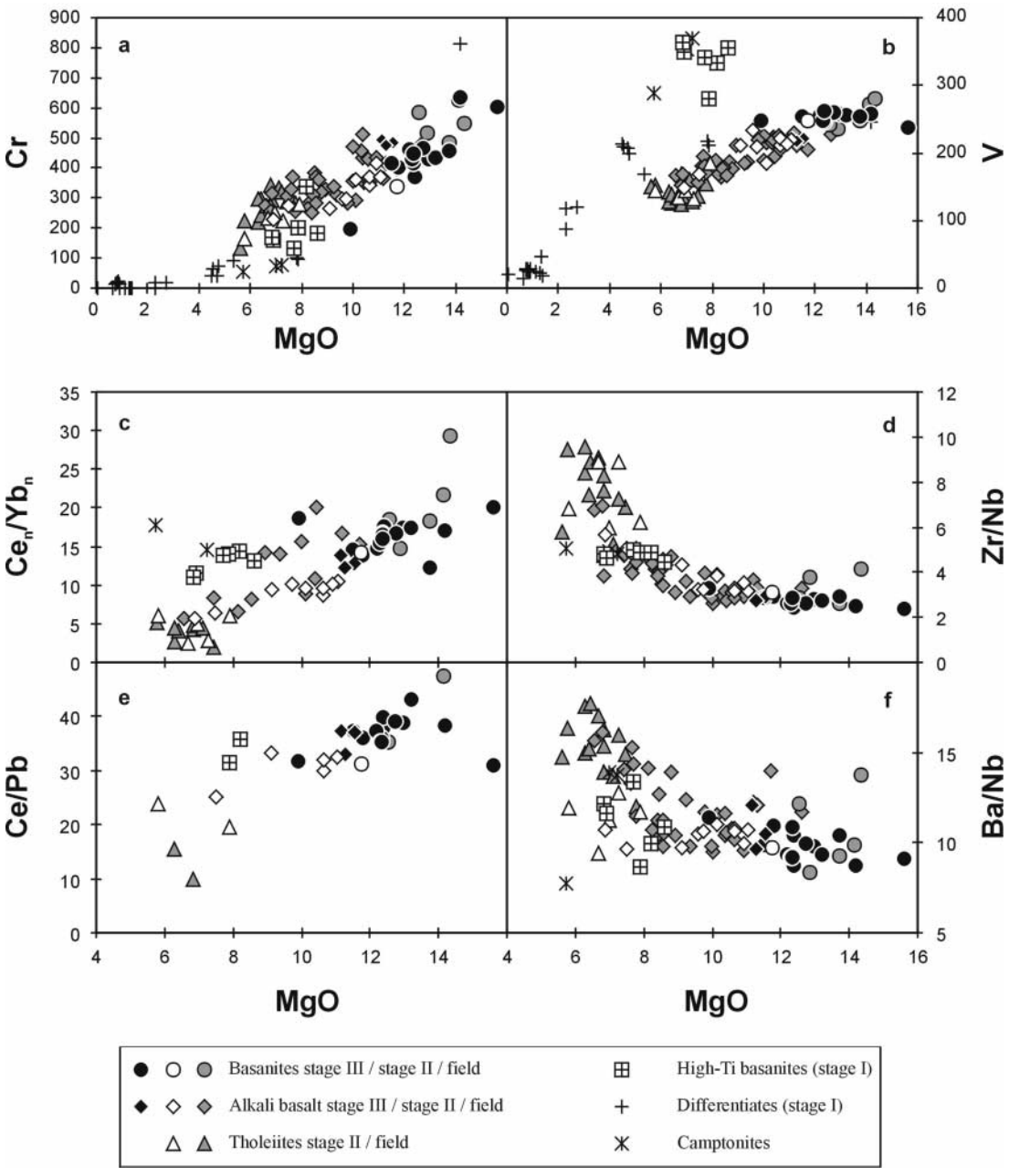

Fig. 4. MgO vs selected trace element concentrations and ratios. Ce_n and Yb_n represent concentrations normalized to chondrite.

HFSE only. All Hf and Ta concentrations reported in this study (Table 1) were determined following this modified procedure. For Zr and Nb only XRF data are reported. However, ICP-MS data for these elements for samples dissolved in HNO_3–HCl–HF were in much better agreement with XRF data than the results for HNO_3 dissolutions. Reproducibility (2σ) was better than 10% over the entire measurement period for all elements except Li, Sc and Rb. Representative analyses of Vogelsberg samples are given in Table 1. A complete dataset is available as an Electronic Appendix at the *Journal of Petrology* website at http://www.petrology.oupjournals.org.

Sr, Nd and Pb isotopic compositions of selected samples (Table 2) were determined on a Finnigan MAT 262RPQ+. Sr and REE were separated on 200–400 mesh AG50WX8 columns, using 2·6N and 6N HCl. Separation of Nd from the REE fraction was carried out on HDEHP columns with a 0·18N HCl elutant. Before dissolution, the sample powder was leached for

Table 1: Major and trace element concentrations of representative samples

Sample no.:	VB96-08	VB96-14	VB96-23	VB96-26	VB96-52	VB97-100	VB97-101	VB97-104	VB97-115
Location:	FBV	FBV	FBV	FBV	FBV	Taufstein	Ortenberg	Dauernheim	Breungesh
Depth (m):	20·86	49·88	77·10	94·40	252·69				
Rock type:	basanite	basanite	basanite	basanite	basanite	basanite	basanite	basanite	basanite
SiO_2	41·12	42·20	43·29	42·76	43·27	40·30	43·30	40·50	43·20
TiO_2	2·56	2·39	2·42	2·56	2·40	2·58	2·62	2·70	2·85
Al_2O_3	12·69	12·32	12·69	12·60	12·61	11·62	12·27	10·74	11·91
Fe_2O_3	6·43	4·32	3·67	4·26	4·17	4·85	3·42	4·78	2·83
FeO	5·45	7·40	7·71	7·51	7·25	6·32	7·93	6·27	7·30
MnO	0·20	0·19	0·20	0·20	0·18	0·18	0·22	0·19	0·17
MgO	12·01	12·55	12·02	12·12	11·32	12·97	12·51	13·53	12·22
CaO	11·69	12·09	11·52	11·52	11·16	11·65	9·86	12·41	10·97
Na_2O	3·18	1·90	2·84	2·93	2·78	2·52	3·12	2·52	2·98
K_2O	0·76	0·71	1·54	0·95	0·64	0·74	1·35	1·25	2·22
H_2O	2·85	3·31	1·00	1·57	3·50	3·93	1·50	2·67	0·99
P_2O_5	0·79	0·76	0·67	0·72	0·60	0·72	0·61	0·80	0·70
Total	99·72	100·14	99·57	99·71	99·89	98·38	98·70	98·36	98·34
Mg-no.	69	70	70	69	68	72	70	73	72
Li	7·55	6·72	6·57	7·40	6·44	6·29	8·03	5·48	7·48
Be	1·60	1·37	1·41	1·49	1·29	1·74	1·82	1·69	1·79
Sc	29	32	29	28	28	23	25	26	24
V	258	257	255	262	248	248	235	273	242
Cr	371	430	462	446	336	486	515	624	586
Co	57	52	54	59	58	55	59	57	53
Ni	255	226	285	276	248	317	332	349	273
Zn	100	101	96	106	99	89	101	100	87
Ga	17	17	17	18	17	16	16	13	17
Rb	89	99	43	30	24	54	31	44	65
Sr	922	1164	813	909	845	872	762	1167	1040
Y	30	27	29	27	28	25	24	27	26
Zr	212	212	203	219	203	222	255	257	243
Nb	87	76	78	76	65	84	68	102	85
Mo	2·66	3·01	4·28	2·58	2·67	1·33	2·68	1·15	3·84
Sn	2·23	0·58	1·38	1·15	0·64	1·51	1·67	1·89	1·78
Cs	0·90	1·07	0·87	1·06	0·70	0·74	0·93	0·59	0·85
Ba	762	746	727	696	632	775	568	1009	1036
La	63·73	58·95	58·82	57·58	49·14	59·23	46·99	73·47	58·81
Ce	125·37	123·12	118·61	118·41	102·73	116·74	97·12	146·67	119·45
Pr	13·28	13·01	12·22	12·46	11·12	12·60	10·75	15·44	12·81
Nd	50·26	49·89	46·25	48·29	43·37	47·34	41·73	56·20	49·36
Sm	9·55	9·34	8·62	9·16	8·33	8·45	7·96	9·43	8·67
Eu	2·89	2·71	2·71	2·79	2·55	2·96	2·72	3·15	2·93
Gd	7·73	7·22	7·06	7·12	6·72	6·92	6·27	7·59	6·83
Tb	1·06	1·02	1·01	1·01	0·97	1·06	0·99	1·05	0·99
Dy	5·37	5·18	5·40	5·33	5·00	5·09	4·89	4·89	4·84
Ho	0·92	0·94	0·94	0·95	0·91	0·86	0·86	0·86	0·85
Er	2·47	2·46	2·69	2·58	2·47	2·26	2·27	2·26	2·28
Tm	0·33	0·33	0·33	0·32	0·32	0·27	0·29	0·27	0·29
Yb	1·92	1·91	2·16	2·00	1·94	1·71	1·77	1·82	1·75

Table 1: continued

Sample no.:	VB96-08	VB96-14	VB96-23	VB96-26	VB96-52	VB97-100	VB97-101	VB97-104	VB97-115
Location:	FBV	FBV	FBV	FBV	FBV	Taufstein	Ortenberg	Dauernheim	Breungesh
Depth (m):	20·86	49·88	77·10	94·40	252·69				
Rock type:	basanite	basanite	basanite	basanite	basanite	basanite	basanite	basanite	basanite
Lu	0·27	0·29	0·32	0·30	0·29	0·23	0·25	0·24	0·26
Hf	4·60	4·63	4·55	4·95	4·74	5·11	5·46	6·19	5·70
Ta	5·82	4·94	5·44	4·97	4·05	5·32	4·27	6·38	5·23
W	1·71	1·22	4·96	1·08	0·95	0·95	0·96	1·31	1·79
Pb	3·33	3·17	3·18	3·36	3·28				
Th	7·97	7·23	6·98	6·84	6·16	7·65	6·23	8·25	7·00
U	1·81	1·62	1·55	1·58	1·44	1·88	1·63	1·89	1·65

Sample no.:	VB97-117	VB96-16	VB96-18	VB96-28	VB96-40	VB96-57	VB97-102	VB97-103	VB97-112
Location:	Eckmannshain	FBV	FBV	FBV	FBV	FBV	Ortenberg	Bergheim	Londorf
Depth (m):		55·91	64·54	175·93	229·00	264·15			
Rock type:	basanite	alk. basalt	alk. basalt	alk. basalt	alk. basalt	alk. basalt	alk. basalt	alk. basalt	alk. basalt
SiO_2	41·50	44·91	45·14	48·25	45·54	50·75	46·20	45·90	50·60
TiO_2	3·09	2·22	2·23	2·39	2·23	2·08	2·13	2·01	2·42
Al_2O_3	10·60	12·58	12·95	13·65	13·05	14·04	13·33	12·95	13·15
Fe_2O_3	3·76	6·57	2·95	4·58	3·77	4·82	1·87	3·39	3·63
FeO	7·25	5·34	8·77	6·57	7·89	5·57	9·73	8·00	6·61
MnO	0·19	0·18	0·18	0·15	0·18	0·14	0·17	0·17	0·15
MgO	14·09	10·94	11·16	8·97	10·79	7·30	9·83	9·72	8·34
CaO	11·93	10·92	10·53	9·01	10·31	7·97	9·63	10·35	7·91
Na_2O	2·58	2·69	3·26	3·27	2·34	3·51	2·45	2·78	3·43
K_2O	2·47	1·26	1·30	1·01	1·04	0·96	1·39	1·01	1·24
H_2O	1·36	1·72	1·20	1·94	2·88	2·58	1·23	1·43	0·99
P_2O_5	0·69	0·51	0·52	0·47	0·49	0·37	0·42	0·79	0·34
Total	99·50	99·83	100·19	100·26	100·50	100·07	98·38	98·51	98·80
Mg-no.	74	67	67	64	67	61	64	65	64
Li	5·38	6·73	7·45	6·26	6·30	4·45	6·63	7·34	9·09
Be	1·63	1·10	1·25	1·10	1·03	1·06	1·12	1·30	1·09
Sc	22	26	29	27	27	21	25	23	16
V	280	222	217	211	220	169	215	189	174
Cr	549	495	473	263	368	272	294	356	386
Co	58	57	61	48	52	41	56	56	47
Ni	340	288	279	149	248	126	203	228	245
Zn	98	143	111	112	108	115	107	115	118
Ga	21	18	18	19	18	20	21	18	20
Rb	71	41	43	22	39	23	32	28	32
Sr	1272	727	661	580	721	412	622	895	559
Y	26	25	25	23	26	28	25	27	24
Zr	317	169	167	161	151	157	147	161	149
Nb	76	56	61	37	48	31	38	62	43
Mo	2·51		3·40	1·10	1·89	1·48	1·41	2·76	1·21
Sn	2·01	0·81	1·47	1·20	0·80	1·00	1·15	1·69	1·11

Sample no.:	VB97-117	VB96-16	VB96-18	VB96-28	VB96-40	VB96-57	VB97-102	VB97-103	VB97-112
Location:	Eckmannshain	FBV	FBV	FBV	FBV	FBV	Ortenberg	Bergheim	Londorf
Depth (m):		55·91	64·54	175·93	229·00	264·15			
Rock type:	basanite	alk. basalt	alk. basalt	alk. basalt	alk. basalt	alk. basalt	alk. basalt	alk. basalt	alk. basalt
Cs	0·54	0·54	0·67	0·31	0·59	0·20	0·36	0·47	0·23
Ba	1047	678	588	359	514	300	439	588	447
La	78·51	44·60	42·19	27·74	34·45	21·54	29·38	60·11	22·43
Ce	169·49	87·10	86·21	60·08	73·43	48·75	63·79	117·24	52·54
Pr	18·23	8·96	8·75	6·67	8·07	5·68	7·38	12·18	5·65
Nd	67·82	36·46	34·26	28·13	32·93	24·18	29·27	43·47	24·35
Sm	11·20	7·75	6·83	6·65	6·93	6·20	6·33	7·88	5·80
Eu	3·51	2·32	2·23	2·18	2·15	2·02	2·21	2·67	2·02
Gd	8·72	6·07	6·01	5·55	5·71	5·53	5·28	6·72	4·87
Tb	1·13	0·88	0·90	0·84	0·89	0·95	0·88	1·04	0·81
Dy	5·21	4·85	4·66	4·57	4·80	4·97	4·52	4·95	4·21
Ho	0·86	0·84	0·83	0·82	0·88	0·90	0·85	0·89	0·77
Er	2·25	2·31	2·34	2·27	2·39	2·47	2·40	2·55	2·14
Tm	0·27	0·30	0·31	0·26	0·32	0·32	0·30	0·32	0·28
Yb	1·56	1·69	1·88	1·71	1·90	2·04	1·93	2·02	1·73
Lu	0·24	0·25	0·26	0·25	0·28	0·29	0·27	0·29	0·25
Hf	7·18		3·78	4·13	3·54	3·72	3·79	3·94	3·68
Ta	5·25		4·15	2·42	3·26	2·06	2·50	3·43	2·98
W	1·45		1·58	0·39	0·89	1·60	0·74	2·06	1·06
Pb		2·33	2·62	1·81	2·27	1·95			
Th	5·88	5·18	5·25	3·24	4·06	2·85	3·00	6·92	2·97
U	1·71	1·27	1·27	0·81	0·95	0·77	0·80	1·71	0·64

Sample no.:	2548	2553	2693	2695	2700	2710	VB96-27	VB96-41	VB97-105	VB97-109
Location:	Geilshausen	Hoherstein	Scharberg	Kloßkopf	Spielberg	Bergheim	FBV	FBV	Dauernheim	Steinkaute
Depth (m):							156·49	234·42		
Rock type:	alk. basalt	alk. basalt	alk. basalt	alk. basalt	alk. basalt	alk. basalt	tholeiite	tholeiite	tholeiite	tholeiite
SiO_2	50·50	49·60	50·00	47·00	49·50	45·90	50·27	52·56	53·80	52·40
TiO_2	1·96	2·60	2·20	2·28	2·22	1·99	2·01	2·02	1·68	2·42
Al_2O_3	13·70	13·10	13·40	13·70	13·20	13·00	14·19	14·93	14·37	13·58
Fe_2O_3	3·74	2·00	3·28	2·61	2·66	3·57	6·39	5·75	4·09	3·18
FeO	5·70	8·10	6·90	8·20	7·40	7·70	4·45	4·35	5·74	7·03
MnO	0·12	0·15	0·16	0·17	0·14	0·17	0·14	0·09	0·10	0·14
MgO	7·09	10·40	7·94	8·78	8·38	10·13	7·72	5·68	6·09	6·65
CaO	7·58	8·90	8·38	10·28	8·35	10·07	8·28	7·77	6·86	7·54
Na_2O	3·30	3·50	3·42	3·44	3·25	2·84	3·38	3·76	3·42	3·41
K_2O	1·34	1·46	1·39	1·42	1·45	1·06	0·50	0·73	0·33	0·88
H_2O	2·80	0·40	1·10	0·80	1·90	2·20	2·75	2·83	2·03	1·13
P_2O_5	0·37	0·42	0·41	0·50	0·41	0·79	0·29	0·33	0·19	0·24
Total	98·20	100·63	98·58	99·18	98·85	99·42	100·37	100·79	98·70	98·60
Mg-no.	62	69	63	64	64	66	61	56	58	59
Li	7·55	9·36	10·27	8·76		8·42	6·26	4·61	7·57	7·07
Be	1·12	1·22	1·18	1·24		1·24	0·85	0·99	0·68	0·97
Sc	17	21	19	24	23	22	24	21	19	15

Table 1: continued

Sample no.:	2548	2553	2693	2695	2700	2710	VB96-27	VB96-41	VB97-105	VB97-109
Location:	Geilshausen	Hoherstein	Scharberg	Kloßkopf	Spielberg	Bergheim	FBV	FBV	Dauernheim	Steinkaute
Depth (m):							156·49	234·42		
Rock type:	alk. basalt	alk. basalt	alk. basalt	alk. basalt	alk. basalt	alk. basalt	tholeiite	tholeiite	tholeiite	tholeiite
V	157	220	189	212	186	194	184	145	143	169
Cr	304	510	337	329	359	350	278	163	219	342
Co	36	47	48	45	42	45	49	36	34	49
Ni	122	290	157	163	169	234	141	82	108	151
Zn	115	130	121	116	120	115	119	125	114	130
Ga	21	—	21	19	17	18	21	22	18	20
Rb	36	35	30	39	37	29	6·58	19	11	21
Sr	514	680	585	736	613	881	456	504	342	423
Y	27	22	26	26	28	26	23	25	21	29
Zr	156	180	172	183	159	159	118	136	87	124
Nb	33	57	37	59	37	58	19	20	9·07	26
Mo		1·81					0·92	1·42	0·99	1.58
Sn	1·08	1·74	0·73	1·26		1·72	1·25	1·15	0·48	1·01
Cs	0·28	0·45	0·72	1·09		0·82	0·20	0·28	0·43	0·74
Ba	464	590	523	614	902	614	223	238	136	362
La	26·63	32·10	29·37	39·21		63·66	16·25	15·96	7·61	13·20
Ce	53·36	68·27	58·15	78·44		118·49	36·91	37·76	17·70	30·84
Pr	6·41	7·62	7·28	9·44		12·31	4·48	4·53	2·47	3·89
Nd	26·50	30·36	26·91	35·11		45·17	20·54	21·22	12·81	19·23
Sm	6·18	6·44		8·52		9·35	5·51	5·79	4·56	5·64
Eu	2·03	2·12	2·48	2·42		2·58	1·87	1·93	1·86	2·03
Gd	5·06	5·69	6·40	7·35		8·30	4·85	5·10	4·04	5·03
Tb	0·85	0·87	0·87	1·04		1·01	0·79	0·79	0·71	0·92
Dy	4·50	4·42	5·30	4·53		5·76	4·25	4·35	4·17	4·84
Ho	0·84	0·80	0·88	0·84		0·97	0·77	0·79	0·73	0·90
Er	2·34	2·13	2·39	2·29		2·36	2·08	2·09	2·04	2·38
Tm	0·28	0·28	0·26	0·21		0·33	0·28	0·27	0·28	0·32
Yb	1·71	1·71	2·38	1·48		1·59	1·66	1·68	1·79	1·92
Lu	0·26	0·25	0·26	0·25		0·30	0·25	0·25	0·23	0·28
Hf		4·13					2·92	3·20	2·56	3·45
Ta		4·00					1·68	1·52	0·77	1·80
W		1·04					0·55	1·00	1·05	1·00
Pb							1·89	1·58		
Th	3·72	3·99	3·41	5·33		6·46	2·15	2·06		1·69
U	0·83	0·85	0·54	1·47		1·86	0·00	0·49	0·23	0·44

Sample no.:	VB97-114	2544	2546	2547	VB96-89	VB98-135	VB98-145	VB96-74	VB96-68	11309
Location:	Londorf	Steinaubach	Rockenberg	Glauberg	FBV	Hasselborn	Rainrod	FBV	FBV	Brg. 57 Staden
Depth (m):					557·00	460·00	290·90	448·00	371·00	86·45
Rock type:	tholeiite	tholeiite	tholeiite	tholeiite	high-Ti	high-Ti	high-Ti	hawaiite	trachyte	camptonite
SiO_2	54·30	53·10	52·50	52·00	45·15	41·60	41·80	47·19	58·92	40·60
TiO_2	1·95	1·40	2·51	2·82	3·28	3·96	4·24	3·11	0·70	3·53
Al_2O_3	14·22	14·50	13·70	14·30	13·84	13·90	13·50	16·52	18·90	13·40

Sample no.:	VB97-114	2544	2546	2547	VB96-89	VB98-135	VB98-145	VB96-74	VB96-68	11309
Location:	Londorf	Steinaubach	Rockenberg	Glauberg	FBV	Hasselborn	Rainrod	FBV	FBV	Brg. 57 Staden
Depth (m):					557·00	460·00	290·90	448·00	371·00	86·45
Rock type:	tholeiite	tholeiite	tholeiite	tholeiite	high-Ti	high-Ti	high-Ti	hawaiite	trachyte	camptonite
Fe_2O_3	3·38	3·88	2·32	3·17	6·25	5·73	4·51	4·70	3·62	5·48
FeO	6·48	5·60	7·60	7·70	5·96	5·59	9·24	6·25	0·33	6·52
MnO	0·13	0·17	0·14	0·13	0·17	0·16	0·17	0·17	0·15	0·20
MgO	6·72	7·22	6·95	5·63	7·63	6·49	8·33	4·68	1·37	6·72
CaO	6·75	7·27	7·50	7·31	9·70	11·99	10·49	8·39	2·48	11·84
Na_2O	3·61	3·21	3·42	3·49	3·42	3·23	2·96	4·24	5·53	1·77
K_2O	0·64	0·39	0·96	0·39	0·85	0·88	0·90	1·92	5·01	2·36
H_2O	0·86	2·30	1·20	1·30	3·08	2·39	2·09	1·58	2·56	2·68
P_2O_5	0·26	0·14	0·25	0·43	0·63	0·49	0·60	0·77	0·18	0·56
Total	99·30	99·17	99·05	98·66	99·96	96·42	98·84	99·52	99·76	99·10
Mg-no.	60	62	60	53	58	56	57	48	44	55
Li	6·06	6·29	8·82	8·17	7·61	6·09	7·43	8·24	17·56	16·05
Be	1·00	0·60	0·83	0·97	1·79	1·39	1·54	1·99	3·44	1·48
Sc	19	21	23	22	27	29	22	18	—	32
V	137	137	161	153	280	349	356	200	18	369
Cr	293	289	334	223	203	161	181	72	—	79
Co	35	43	39	35	46	52	52	28	—	45
Ni	153	159	160	95	118	131	75	32	—	47
Zn	129	118	140	152	121	85	108	126	105	181
Ga	17	18	23	23	23	18	22	21	25	22
Rb	16	12	19		26	18	10	18	152	69
Sr	502	347	420	563	831	784	780	1169	496	819
Y	24	19	26	28	26	23	24	31	26	29
Zr	122	69	126	151	292	230	231	322	500	241
Nb	16	10	24	16	60	50	52	75	116	50
Mo	1·44				2·84		2·15			
Sn	0·81	0·39	0·67	1·17	1·28	1·27	1·96	2·27	1·93	1·36
Cs	0·34	0·39	0·90	0·15	0·60	0·58	0·66	0·56	1·26	19·49
Ba	246	149	328	261	521	580	564	796	1417	687
La	9·78	6·93	14·38	11·25	44·93	34·54	33·91	58·66	81·87	45·06
Ce	28·49	14·33	29·83	30·00	103·46	80·74	84·53	130·44	151·77	95·23
Pr	3·31	2·09	4·00	4·95	11·89	9·14	9·11	14·80	13·72	11·51
Nd	16·52	11·59	18·81	25·79	45·84	36·39	37·74	57·02	43·61	46·05
Sm	4·90			7·35	9·19	7·96	7·26	11·02	6·76	9·09
Eu	1·75	2·17	2·17	2·49	2·78	2·93	2·72	3·31	1·92	2·89
Gd	4·19	3·95	5·50	5·63	7·48	6·27	6·88	8·72	5·00	6·99
Tb	0·77	0·60	0·95	0·97	1·09	0·97	1·00	1·22	0·72	1·08
Dy	4·03	4·34	5·78	4·93	5·41	4·83	5·12	6·16	3·92	5·13
Ho	0·76	0·63	0·83	0·88	0·96	0·82	0·92	1·06	0·76	0·93
Er	2·08	1·74	2·82	2·35	2·48	2·09	2·24	2·75	2·15	2·52
Tm	0·26	0·25	0·33	0·29	0·32	0·31	0·28	0·35	0·33	0·31
Yb	1·59	1·89	1·83	1·58	2·00	1·88	1·72	2·14	2·20	1·75
Lu	0·23	0·23	0·29	0·24	0·29	0·24	0·25	0·31	0·34	0·26
Hf	3·26				7·10	5·52	5·47			
Ta	1·10				4·22	3·76	3·80			
W	1·38				1·48	1·52	1·08			
Pb					3·28			3·65	10·20	

Table 1: continued

Sample no.:	VB97-114	2544	2546	2547	VB96-89	VB98-135	VB98-145	VB96-74	VB96-68	11309
Location:	Londorf	Steinaubach	Rockenberg	Glauberg	FBV	Hasselborn	Rainrod	FBV	FBV	Brg. 57 Staden
Depth (m):					557·00	460·00	290·90	448·00	371·00	86·45
Rock type:	tholeiite	tholeiite	tholeiite	tholeiite	high-Ti	high-Ti	high-Ti	hawaiite	trachyte	camptonite
Th	1·27		1·78		5·00	3·24	3·33	6·35	17·51	4·47
U	0·31		0·64	0·22	1·36	0·91	1·56	1·69	4·58	1·19

Major and minor oxides and the trace elements Sc, V, Cr, Co, Ni, Zn, Ga, Rb, Sr, Y, Zr, Nb and Ba were analysed by XRF, others by ICP-MS. Mg-number calculated using FeO = 0·85 FeO*.

2 h at 80°C in 2 ml of 2·6N HCl. The leachate was removed, and the remaining powder was washed twice with 1 ml of H_2O. Then the powder was dissolved and treated as above. Several samples were also dissolved, separated and measured without prior leaching. For these samples both leached and unleached values are given in Table 2. Nd samples were loaded on Re double filaments in dilute HNO_3 and H_3PO_4 and measured on the mass spectrometer. Measurements were run until 120 ratios were measured or the error was better than 0·000010 (2σ). Sr samples were loaded on Re double or Ta single filaments in dilute H_3PO_4. Measurements where stopped after 120 ratios or at an error better than 0·000020 (2σ).

The La Jolla Nd standard gave an average value of 0·511839 ± 14 ($n = 16$). Nd measurements were corrected by +0·000019 to achieve the recommended value of 0·511858. The NBS-987 gave an average of 0·710270 ± 39 ($n = 14$), but 0·710289 ± 08 for measurements before September 1998 ($n = 6$) and 0·710256 ± 24 for measurements after that time. Measurements were accordingly corrected by –0·000039 before September 1998, and by –0·000006 after that time, to obtain the recommended value of 0·710250. Blanks were significantly below 1 ng for Sr, with an average of ~500 pg. Nd blanks were lower than 500 pg, with an average of ~200 pg.

For Pb-isotope analyses, samples were leached for 30 min in cold 2·6N HCl and subsequently dissolved in a 1:1 HF–HNO_3 mixture at 200°C in a Teflon pressure bomb. The solution was dried down and dissolved in 6N HCl twice. Then it was dried down and dissolved in 0·5N HBr, dried down again and finally dissolved in 1 ml of 0·5N HBr. Of the resulting solution, two 0·5 ml splits were separated and measured independently. Pb separation was carried out on 100 ml Teflon columns with 200–400 mesh, Biorad AG1-X8 resin, using 0·5N HBr, 2N HCl and 6N HCl as elutant. The samples were passed through the columns, dried down, taken up in 0·5N HBr, dried down again and finally taken up in 0·5 ml of 0·5N HBr. This solution was passed through the separation columns once more to clean the separate. The Pb samples were loaded on Re single filaments with silica gel and dilute H_3PO_4. Measurements were run for 90 ratios, or until the error in $^{207}Pb/^{204}Pb$ was better than 0·005 (2σ).

Blanks were lower than 385 pg, with an average of 230 pg. Reproducibility was better than 0·1% per a.m.u. over the entire measuring period, based on repeated measurements of the NBS-981 standard, but usually better than 0·03% per a.m.u. over a single measuring day. Performing the mass fractionation correction using the measured standard values for the same day significantly improved the reproducibility of repeated measurements on single samples over several days as well. Mass fractionation correction factors are 0·01–0·13% per a.m.u. Estimated reproducibilities of single samples are better than 0·05% per a.m.u.

All determined isotopic compositions are given in Table 2. Age corrections for Pb isotope ratios are insignificant with respect to the variation in the samples and therefore not shown in Table 2 and Fig. 7 (below).

Further details on analytical procedures have been given by Bogaard (2000).

SAMPLE DESCRIPTION

Petrography

All studied rocks have porphyritic textures. High-Ti basanites (Stage I), alkali basalts (Stage II) and basanites (Stage III) contain varying amounts of olivine phenocrysts and sub- to euhedral Ti-augite phenocrysts with oscillatory zoning patterns. The fine-grained groundmass consists of plagioclase, clinopyroxene, olivine and Ti-magnetite. In high-Ti basanites, clinopyroxene is the dominant groundmass phase. Ehrenberg & Hickethier (1978) described hornblende basalts that have similar major element compositions to the high-Ti basanites (high Ti contents, relatively low MgO). These rocks contain significant amounts of hornblende phenocrysts, in addition to

augite and olivine. Similar rocks are also found in the Rhön (Ehrenberg & Hickethier, 1994). Basanites from Stage III commonly contain peridotite inclusions of up to several centimetres in size.

Tholeiites contain both clinopyroxene and sub- to euhedral orthopyroxene (pigeonite) phenocrysts. The groundmass of tholeiites is composed of plagioclase, clinopyroxene, Ti-magnetite and accessory apatite. Olivine is rarely observed as groundmass phase.

Hawaiites, mugearites, latites and trachytes in addition to clinopyroxene commonly contain hornblende and plagioclase or (for trachytes) alkali feldspar phenocrysts in a groundmass that predominantly consists of plagioclase. Clinopyroxenes occur both as Ti-augites with oscillatory zoning patterns and as phenocrysts with light green cores.

Camptonites are strongly porphyritic and contain euhedral, up to 2 cm large hornblende and augite phenocrysts. In addition, sample 11175 contains up to 4 mm large biotite phenocrysts. The groundmass consists of plagioclase, alkali feldspar, hornblende, Fe–Ti oxides and accessory biotite.

Chemical alteration

Bogaard *et al.* (2001*a*) showed that chemical alteration even in the most strongly weathered parts of basalt flows in the FBV '96 borehole is relatively limited. However, alkalis (K, Na, Rb) may be mobilized even in apparently fresh rocks as a result of breakdown of interstitial groundmass glass (mesostasis) and subsequent formation of analcime and/or zeolites. Rb concentrations vary widely in Vogelsberg basanites and are not correlated with other incompatible elements. Na_2O and K_2O also show relatively strong scatter with respect to SiO_2 and MgO in basanites and tholeiites, respectively. Furthermore, water concentrations are >2 wt % in many of the analysed samples (Table 1), which is usually seen as an indicator of alteration.

Despite these observations, the overall coherent variation of most major and trace elements appears to justify the conclusion that chemical alteration is not a major problem for elements other than mobile alkalis.

Major and compatible trace elements

Basanites (SiO_2 42–45 wt %) have high MgO (11–15 wt %) and compatible trace element contents (Table 1, Figs 3 and 4). TiO_2 concentrations are moderately high (2·3–2·8 wt %). Alkali basalts (SiO_2 45–53·5 wt %) have lower MgO (6·5–11·5 wt %) and compatible trace element contents that decrease with increasing SiO_2. Most of the basalts with $SiO_2 > 50$ wt % plot very close to the alkali basalt–tholeiite dividing line of MacDonald (1968; Fig. 3a). Tholeiites (SiO_2 51·5–56 wt %) have MgO contents of 5·6–7·9 wt % and low compatible trace element concentrations. They have variable but generally low K_2O contents (0·3–1·0 wt %), which are lower than those found in most alkali basalts (0·7–1·7 wt %). Basanites, alkali basalts and tholeiites form a continuous trend with decreasing MgO, TiO_2, CaO and P_2O_5 and increasing Al_2O_3 and Na_2O with increasing SiO_2 (Fig. 3).

The high-Ti basanites of the first stage have much higher TiO_2 (3·4–4·4 wt %) and lower MgO (6·8–8·6 wt %), Ni and Cr than 'normal' basanites, but similar CaO, Sc and alkalis and higher V (Table 1; Figs 3 and 4). High-Ti basanites and differentiates (hawaiites–trachytes) plot on a continuous trend where alkalis and Al_2O_3 increase and MgO, TiO_2, FeO*, CaO and compatible trace element concentrations strongly decrease with increasing SiO_2. The composition of differentiates is typical for formation by fractional crystallization of parental magmas similar to high-Ti basanites at mid- or upper-crustal levels (Bogaard *et al.*, 2001*b*).

Trace elements

Basanites and primitive alkali basalts show strong enrichment of moderately and highly incompatible elements (Ce_n/Yb_n 12–30, Fig. 4). K and Pb are strongly depleted compared with elements of similar compatibility. Th, U, Zr and Ti also are slightly depleted compared with neighbouring elements (Fig. 5a). Apart from these anomalies, mantle-normalized concentrations increase regularly with increasing incompatibility and show typical intraplate or ocean-island basalt (OIB) patterns.

Alkali basalts (Ce_n/Yb_n 5·6–20) and tholeiites (Ce_n/Yb_n 2·0–6·0) are less enriched in incompatible trace elements. The characteristic negative anomalies (Th, U, K, Pb, Zr, Ti) of the basanite patterns are less pronounced in alkali basalts. The most depleted tholeiites show increasing normalized concentrations from Yb to Eu, similar to basanites. From Eu to Rb the patterns are rather flat, except for a strong negative Zr anomaly and positive Sr and Ba anomalies (Fig. 5c). Ratios of Zr/Nb (4·8–9·6) are much higher and Ce/Pb (8–24) is lower than is typical for basanites. Furthermore, the Ba/Nb ratio (9–18) shows considerable overlap with basanites, but reaches much higher maximum values. Alkali basalts are intermediate between basanites and tholeiites in most major and trace element variation plots (Figs 3 and 4) and in trace element ratios.

Trace element patterns of high-Ti basanites (Fig. 5d) are similar to those of normal basanites. However, HFSE (especially Ti) are enriched, whereas highly incompatible elements are less enriched (Ce_n/Yb_n 11–14) in the high-Ti basanites. Ce/Pb is similar to normal basanites, but Zr/Nb (4·4–5·0) is higher and Ba/Nb (8·7–13·4) reaches higher maximum values in

high-Ti basanites (Fig. 4). Camptonites have very similar Ti concentrations and Ce_n/Yb_n, Zr/Nb and Ba/Nb to high-Ti basanites (Fig. 4).

Radiogenic isotopes

Most basanites and primitive alkali basalts have $^{87}Sr/^{86}Sr$ (0·7031–0·7036), $^{143}Nd/^{144}Nd$ (0·51271–0·51295) and Pb isotopic compositions ($^{206}Pb/^{204}Pb$ 19·27–19·42; $^{207}Pb/^{204}Pb$ 15·60–15·67; $^{208}Pb/^{204}Pb$ 38·94–39·41) close to those of the European Asthenospheric Reservoir (EAR) and Low Velocity Component (LVC) compositions (Cebriá & Wilson, 1995; Hoernle *et al.*, 1995; Figs 6 and 7). The tholeiites have Sr and Nd isotopic ratios that fall below a line between asthenospheric (EAR, LVC) and Bulk Silicate Earth (BSE; Fig. 6). In contrast to the tholeiites, alkali basalts lie close to this line, generally having higher $^{143}Nd/^{144}Nd$ for a given value of $^{87}Sr/^{86}Sr$. Pb isotopic compositions for tholeiites and evolved alkali basalt ($^{206}Pb/^{204}Pb$ 18·56–19·13; $^{207}Pb/^{204}Pb$ 15·59–15·63; $^{208}Pb/^{204}Pb$ 38·22–38·82) are more unradiogenic than the primitive basanites. On a plot of $^{206}Pb/^{204}Pb$ vs $^{208}Pb/^{204}Pb$, the Vogelsberg volcanic rocks form a highly linear array parallel to the Northern Hemisphere Reference Line (NHRL; Hart, 1984), which extends from the EAR composition to much more unradiogenic values (Fig. 7b). Mafic volcanic rocks from the East and West Eifel define a similar array except for its distinctly higher $^{208}Pb/^{204}Pb$ ratio. $^{207}Pb/^{204}Pb$ is very similar in all analysed volcanic rocks from both the Eifel and the Vogelsberg regions (Fig. 7a).

Three high-Ti basanites have almost identical isotopic compositions. $^{87}Sr/^{86}Sr$ is similar but $^{143}Nd/^{144}Nd$ significantly lower (0·512775 ± 15) compared with normal basanites. Pb isotopic compositions fall in the range of normal basanites ($^{206}Pb/^{204}Pb$ 19·29–19·35; $^{208}Pb/^{204}Pb$ 38·99–39·12). One camptonite has higher $^{87}Sr/^{86}Sr$ (0·7038) than the high-Ti basanites but similar $^{143}Nd/^{144}Nd$ (0·51283) to them.

Tertiary nephelinites to tholeiites from the Northern Hessian Depression have similar trace element and Sr and Nd isotopic compositions to the Vogelsberg rocks (Fig. 6a). Primitive mafic rocks from the Quaternary East and West Eifel have a similar range in $^{143}Nd/^{144}Nd$ to the Vogelsberg rocks, but have higher $^{87}Sr/^{86}Sr$ and are thus displaced to the right of the Vogelsberg field (Fig. 6a). The Eifel rocks form a linear array that extends from the EAR/LVC to BSE.

FRACTIONAL CRYSTALLIZATION

High compatible trace element (Ni, Cr, Sc, V) concentrations, high Mg-number and the common occurrence of mantle xenoliths suggest that the basanites may be close to primary mantle melts. Alkali basalts and tholeiites have lower Mg-number and Ni, Cr, Sc and V concentrations (Fig. 4, Table 1) and do not contain mantle xenoliths. These magmas also have higher SiO_2 and therefore are likely to have fractionated significant amounts of clinopyroxene, olivine (alkali basalts, basanites), orthopyroxene (tholeiites) and Fe–Ti oxides. The positive Sr anomalies and lack of negative Eu anomalies in the tholeiites argue against significant plagioclase fractionation. Therefore, fractional crystallization probably took place at depths >15 km, possibly at the crust–mantle boundary (Wittenbecher, 1992; Jung & Masberg, 1998).

Incompatible trace element concentrations systematically decrease with decreasing MgO from basanites to alkali basalts to tholeiites. Tholeiites and alkali basalts thus cannot be derived from basanitic parent magmas by fractional crystallization. Rather, tholeiites are likely to be melts from a mantle source that is depleted relative to the source of the basanites. The relatively low incompatible trace element contents and evidence for fractional crystallization make it likely that the tholeiites were also affected by crustal contamination. This is considered in the next section.

Despite their low SiO_2 contents, high-Ti basanites have low Mg-number (54–58) and Ni (75–150 ppm) and Cr (130–340 ppm) contents. These values suggest that high-Ti basanites may have undergone significant amounts of fractional crystallization. However, in addition to their high TiO_2 and Al_2O_3 contents, high-Ti basanites have similar Sc to normal basanites and significantly higher V concentrations than them (Fig. 4). Ehrenberg & Hickethier (1978) described petrographically very different hornblende basalts from drill cores in the southern part of the Vogelsberg that have very similar major element characteristics to the high-Ti basanites. Similar rocks are found in the Rhön (Ehrenberg & Hickethier, 1994). The Cretaceous camptonites are also strongly amphibole and biotite phyric and also have similar major and trace element characteristics to the high-Ti basanites. Finally, high-Ti basanites, camptonites and hornblende basalts from the Rhön (Jung & Hoernes, 2000) have significantly and consistently higher Zr/Nb ratios than 'normal' basanites (Fig. 4).

The above evidence suggests that the high-Ti basanites could represent partial melts of a different mantle source than that of normal basanites. 'Primary' Mg-number and Ni and Cr concentrations are the result of buffering by olivine and orthopyroxene in the melt residue. However, if melting takes place in highly metasomatized mantle, and the melt residue is no longer harzburgitic, primary (that is, unfractionated) melts might have much lower Mg-number and Ni and Cr concentrations. This does not imply that high-Ti

Table 2: Sr, Nd and Pb isotopic compositions

Sample	Rock type	*	$^{87}Sr/^{86}Sr$	2σ	$^{87}Sr/^{86}Sr_i$	$^{143}Nd/^{144}Nd$	2σ	$^{143}Nd/^{144}Nd_i$	ε_0Sr	ε_0Nd	$\Delta\varepsilon Nd$†	‡	$^{206}Pb/^{204}Pb$	2σ	$^{207}Pb/^{204}Pb$	2σ	$^{208}Pb/^{204}Pb$	2σ
VB96-08	basanite	l	0·703209	±14	0·703146	0·512884	±06	0·512844	−18·32	3·98	0·12	1	19·377	±0·0008	15·615	±0·0006	39·131	±0·0016
		u	0·703295	±18		0·512885	±09					2	19·452	±0·0042	15·659	±0·0034	39·331	±0·0097
												Final	19·415	±0·0044	15·637	±0·0045	39·231	±0·0052
VB96-14	basanite	l	0·703286	±12	0·703230	0·512848	±05	0·512816	−17·23	3·28	−0·18							
		u	0·703422	±18		0·512867	±08											
VB96-16	alkali basalt	l	0·703179	±15	0·703142	0·512933	±12	0·512906	−18·75	4·94	1·30							
		u	0·703253	±22		0·512950	±07											
VB96-18	alkali basalt	l	0·703148	±12	0·703106	0·512948	±07	0·512897	−19·19	5·23	1·03	1	19·274	±00015	15·607	±0·0013	38·957	±0·0034
		u	0·703195	±20		0·512934	±06					2	19·267	±0·0029	15·595	±0·0025	38·920	±0·0067
												Final	19·271	±0·0021	15·601	±0·0018	38·939	±0·0021
VB96-23	basanite	l	0·703350	±16	0·703316			0·512822	−16·32	4·32	0·10	1	19·403	±0·0023	15·608	±0·0018	39·144	±0·0046
		u	0·703288	±08		0·512862	±05					Final	19·403	±0·0023	15·608	±0·0018	39·144	±0·0046
VB96-26	basanite	l	0·703277	±12	0·703256	0·512849	±06	0·512803	−17·36	3·30	−0·48							
		u	0·703375	±20		0·512838	±09											
VB96-27	tholeiite	l	0·703179	±13	0·703170			0·512727	−18·75	2·07	−1·90							
		u	0·703179	±13		0·512786	±03											
VB96-28	alkali basalt	l	0·703169	±12	0·703144	0·512857	±11	0·512779	−18·89	3·46	−1·07							
		u	0·703222	±18		0·512830	±06											
VB96-40	alkali basalt	l	0·703262	±12	0·703226	0·512866	±03	0·512820	−17·57	3·63	−0·08	1	19·129	±0·0073	15·598	±0·0060	38·817	±0·0149
		u	0·703329	±20		0·512867	±09					Final	19·129	±0·0073	15·598	±0·0060	38·817	±0·0149
VB96-41	tholeiite	l	0·703164	±11	0·703139	0·512779	±08	0·512715	−18·96	1·94	−2·15	1	18·763	±0·0033	15·588	±0·0028	38·317	±0·0073
		u	0·703189	±19		0·512772	±09					2	18·787	±0·0020	15·586	±0·0017	38·328	±0·0044
												Final	18·775	±0·0018	15·587	±0·0018	38·322	±0·0019
VB96-52	basanite	l	0·703433	±09	0·703414			0·512807	−15·14	3·32	0·12	1	19·357	±0·0049	15·673	±0·0042	39·409	±0·0102
		u	0·703454	±09		0·512850	±06					Final	19·357	±0·0049	15·673	±0·0042	39·409	±0·0102
VB96-57	alkali basalt	l	0·703534	±10	0·703497	0·512771	±08	0·512713	−13·71	1·77	−1·12	1	19·068	±0·0112	15·645	±0·0092	38·794	±0·0225
		u	0·703524	±14		0·512769	±13					2	19·028	±0·0072	15·605	±0·0060	38·685	±0·0148
												Final	19·048	±0·0051	15·625	±0·0052	38·739	±0·0050
VB96-68	trachyte	l	0·703595	±12	0·703381	0·512827	±06	0·512798	−12·84	3·00	0·29							
		u	0·703594	±16		0·512841	±08											
VB96-74	hawaiite	l	0·703377	±10	0·703367	0·512818	±04	0·512779	−15·94	2·81	−0·56							
		u	0·703372	±19		0·512830	±07											

Table 2: continued

Sample	Rock type	*	$^{87}Sr/^{86}Sr$	2σ	$^{87}Sr/^{86}Sr_i$	$^{143}Nd/^{144}Nd$	2σ	$^{143}Nd/^{144}Nd_i$	ε_0Sr	ε_0Nd	$\Delta\varepsilon Nd$†	‡	$^{206}Pb/^{204}Pb$	2σ	$^{207}Pb/^{204}Pb$	2σ	$^{208}Pb/^{204}Pb$	2σ
VB96-89	high-Ti bas.	l	0·703270	±15	0·703273	0·512834	±05	0·512790	−17·45	3·01	−0·53	1	19·341	±0·0021	15·607	±0·0018	39·062	±0·0047
		u	0·703295	±15		0·512842	±09					2	19·365	±0·0053	15·629	±0·0043	39·169	±0·0110
												Final	19·353	±0·0041	15·618	±0·0040	39·116	±0·0040
VB97-100	basanite	l	0·703234	±18	0·703192			0·512858	−17·97	4·31	0·51							
		u	0·703247	±19		0·512901	±10											
VB97-101	basanite	l	0·703371	±16	0·703344	0·512887	±10	0·512833	−16·02	4·04	0·48							
		u	0·703359	±15		0·512878	±09											
VB97-102	alkali basalt	l	0·703472	±11	0·703437			0·512780	−14·59	2·93	−0·16							
		u	0·703443	±11		0·512830	±10											
VB97-103	alkali basalt	l	0·703445	±11	0·703424	0·512868	±13	0·512813	−14·97	3·67	0·27							
		u	0·703419	±18		0·512856	±10											
VB97-104	basanite	l	0·703582	±14	0·703557	0·512839	±11	0·512804	−13·03	3·11	0·43	1	19·264	±0·0022	15·599	±0·0021	38·965	±0·0052
		u	0·703626	±12		0·512843	±07					2	19·268	±0·0018	15·632	±0·0019	39·060	±0·0067
												Final	19·266	±0·0005	15·615	±0·0002	39·012	±0·0010
VB97-105	tholeiite	l	0·703319	±14	0·703298			0·512637	−16·76	0·60	−2·94	1	18·551	±0·0040	15·618	±0·0034	38·185	±0·0086
		u	0·703513	±18		0·512711	±09					2	18·565	±0·0024	15·634	±0·0027	38·255	±0·0091
												Final	18·558	±0·0022	15·626	±0·0012	38·220	±0·0003
VB97-109	tholeiite	l	0·704049	±11	0·704016			0·512602	−6·40	−0·21	−1·57	1	18·864	±0·0016	15·628	±0·0013	38·372	±0·0030
		u	0·704072	±23		0·512669	±04					2	18·872	±0·0013	15·636	±0·0013	38·398	±0·0039
												Final	18·868	±0·0004	15·632	±0·0001	38·385	±0·0006
VB97-112	alkali basalt	l	0·704209	±10	0·704171			0·512628	−4·13	0·04	−0·83							
		u	0·704241	±23		0·512682	±03											
VB97-114	tholeiite	l	0·703771	±18	0·703750	0·512620	±08	0·512573	−10·34	−1·17	−3·36	1	18·568	±0·0017	15·613	±0·0014	38·236	±0·0036
												2	18·567	±0·0017	15·617	±0·0015	38·247	±0·0038
												Final	18·568	±0·0001	15·615	±0·0001	38·242	±0·0001
VB97-115	basanite	l	0·703580	±12	0·703538	0·512803	±08	0·512765	−13·05	2·46	−0·30							
		u	0·703577	±10		0·512809	±08											
VB97-117	basanite	l	0·703473	±08	0·703436	0·512750	±09	0·512723	−14·57	1·59	−1·49							
		u	0·703523	±17		0·512773	±08											
VB98-135	high-Ti bas.	l	0·703341	±08	0·703323	0·512810	±04	0·512761	−16·45	2·54	−0·94	1	19·296	±0·0041	15·625	±0·0033	39·062	±0·0085
												2	19·305	±0·0028	15·629	±0·0025	39·081	±0·0075
												Final	19·300	±0·0017	15·627	±0·0014	39·072	±0·0007

Sample	Rock type	*	$^{87}Sr/^{86}Sr$	2σ	$^{87}Sr/^{86}Sr_i$	$^{143}Nd/^{144}Nd$	2σ	$^{143}Nd/^{144}Nd_i$	ε_0Sr	ε_0Nd	$\Delta\varepsilon Nd$†	‡	$^{206}Pb/^{204}Pb$	2σ	$^{207}Pb/^{204}Pb$	2σ	$^{208}Pb/^{204}Pb$	2σ
VB98-145	high-Ti bas.	l	0·703377	±08	0·703372	0·512825	±04	0·512776	−15·94	2·83	−0·54	1	19·285	±0·0025	15·630	±0·0023	38·983	±0·0065
												2	19·289	±0·0041	15·637	±0·0033	39·004	±0·0405
												Final	19·287	±0·0021	15·633	±0·0017	38·994	±0·0218
2544	tholeiite	l	0·703285	±12	0·703324	0·512741	±04	0·512682	−17·24	1·19	−2·28							
		u	0·703344	±09														
2546	tholeiite	l	0·704036	±11	0·704005	0·512668	±06	0·512607	−6·58	−0·23	−1·63							
		u	0·704074	±08														
2547	tholeiite	l	0·703928	±09	0·703923	0·512663	±03	0·512596	−8·11	−0·33	−2·05							
		u	0·703936	±07														
2548	alkali basalt	l	0·704210	±08	0·704160	0·512602	±07	0·512547	−4·11	−1·52	−2·39							
		u	0·704268	±07														
2553	alkali basalt	l	0·703998	±08	0·703961	0·512750	±03	0·512699	−7·12	11·37	−0·14							
		u	0·704004	±08														
2693	alkali basalt	l	0·703782	±12	0·703746	0·512771	±03	0·512717	−10·19	1·77	−0·38							
2695	alkali basalt	l	0·703401	±13	0·703364	0·512875	±03	0·512827	−15·60	3·80	0·51							
2700	alkali basalt	l	0·703712	±12	0·703669	0·512754	±03	0·512710	−11·18	1·44	−0·92							
2710	alkali basalt	l	0·703457	±16	0·703435	0·512837	±04	0·512790	−14·80	3·06	−0·07							
11309	camptonite	l	0·703805	±11	0·703570			0·512642	−9·86	2·96	0·88							
		u	0·704134	±09		0·512832	±12											

*l, leached; u, unleached.
†See text for calculation and discussion of $\Delta\varepsilon Nd$.
‡1 and 2 are first and second analyses, respectively. Final is final calculated result.

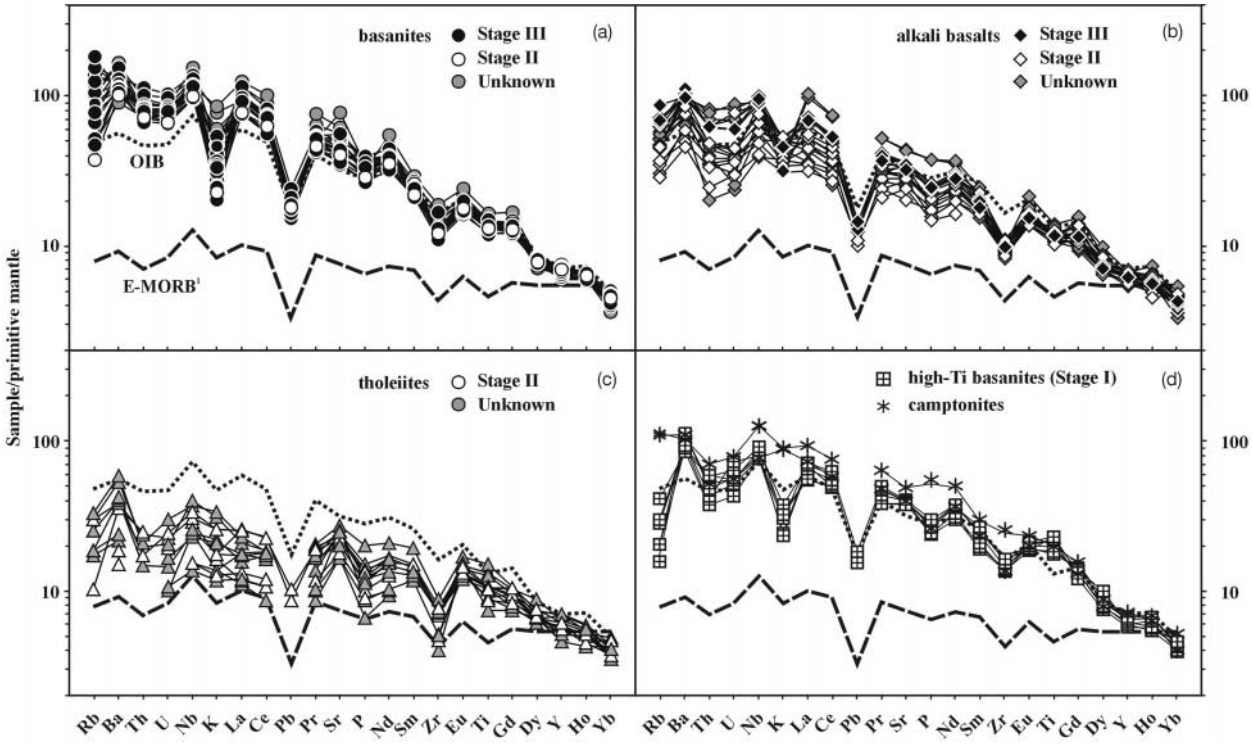

Fig. 5. Primitive mantle normalized trace element concentration diagrams for (a) basanites, (b) alkali basalts, (c) tholeiites and (d) high-Ti basanites and camptonites. Primitive mantle composition and element order after Sun & McDonough (1989). Bold lines representing average OIB and E-MORB (Sun & McDonough, 1989) are shown for comparison.

basanites did not undergo any fractional crystallization. However, it is suggested that they may be much closer to primary melts than would be inferred from their Mg-number and Ni and Cr contents alone. This possibility is further explored below.

CRUSTAL CONTAMINATION

Trace element and isotopic compositions of many continental tholeiites differ from those of oceanic basalts, which has been explained by either an influence of the sub-continental lithospheric mantle (SCLM; Wilson & Downes, 1991; Gallagher & Hawkesworth, 1992; O'Reilly & Zhang, 1995) or lower-crustal contamination (Chesley & Ruiz, 1998; Fitton *et al*., 1998). This long-standing debate shows that these two processes are not easily distinguished (Thirlwall & Jones, 1983; Hawkesworth *et al*., 1984). Telling one from the other requires a firm grasp of the geochemical composition of the local lower crust and lithospheric mantle, in addition to a detailed evaluation of trace element and radiogenic isotope systematics. The available information on the composition of the lower crust of central Germany is therefore briefly reviewed below.

The lower crust of central Germany

The lower crust of central Germany is largely composed of mafic and rare felsic granulites. These appear to be cumulates from basaltic magma that intruded at the crust–mantle boundary (Mengel *et al*., 1991; Sachs & Hansteen, 2000). In the Eifel region, this underplating event took place ~450 Myr ago (Rudnick & Goldstein, 1990). Many mafic granulites show evidence of a later metasomatic overprinting event. Sachs & Hansteen (2000) recently showed that this overprinting is most probably related to Tertiary–Quaternary magmatism. Metasomatism resulted in (1) formation of hydrous phases such as amphibole and biotite under the influence of fluids released from the magmas, and (2) breakdown of earlier hydrous phases closer to the intrusive contact, as a result of heating. The presence of glass (1% or less) in metasomatized xenoliths shows that such heating may have induced small degrees of melting in the lower crust.

Granulites from the Eifel and Massif Central have Sr and Nd isotopic compositions that extend from Bulk Silicate Earth (BSE) values towards lower $^{143}Nd/^{144}Nd$ and higher $^{87}Sr/^{86}Sr$ ratios (Stosch & Lugmair, 1984; Downes & Leyreloup, 1986; Loock *et al*., 1990; Fig. 6c). The highest $^{87}Sr/^{86}Sr$ and lowest $^{143}Nd/^{144}Nd$ ratios are found in felsic granulites, but some mafic Eifel

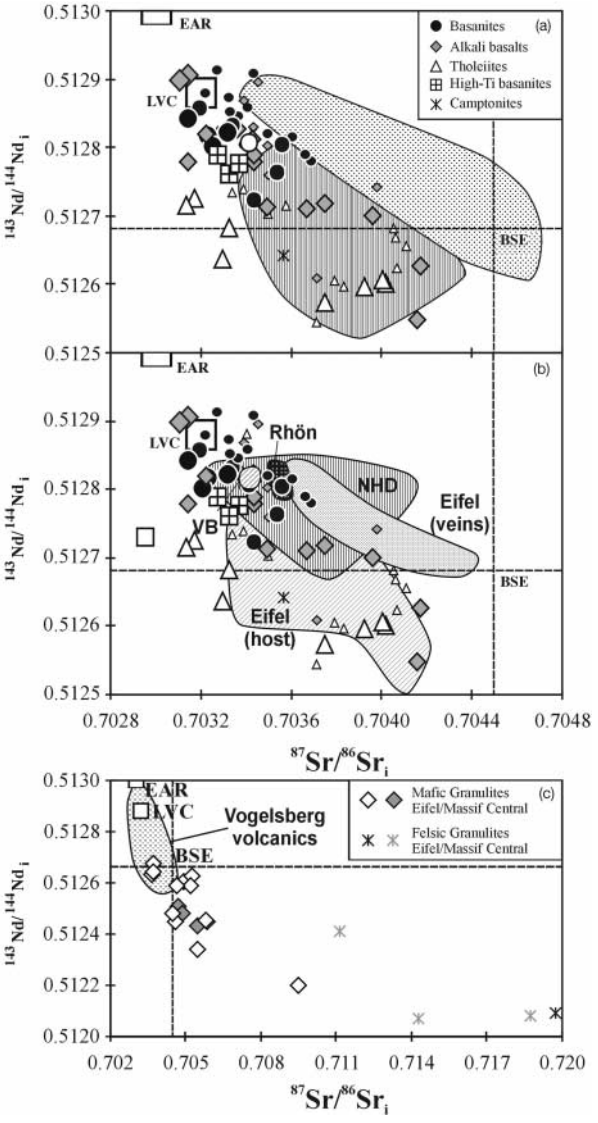

Fig. 6. $^{87}Sr/^{86}Sr$ vs $^{143}Nd/^{144}Nd$ for basic volcanic rocks from the Vogelsberg. Large symbols are from this study; small symbols are from Wittenbecher (1992) and Jung & Masberg (1998). Analytical error is smaller than symbol size. (a) Isotopic variation of Neogene lavas from the Eifel (Wörner *et al*., 1986; stippled) and the Northern Hessian Depression (Wedepohl, 1985; striped). (b) Data from mantle xenolith suites from central Germany; NHD, Northern Hessian Depression (Hartmann & Wedepohl, 1990); VB, Vogelsberg (Witt-Eickschen, 1993); Rhön data from Witt-Eickschen & Kramm (1997); Eifel data from Stosch & Lugmair (1986), Witt-Eickschen & Kramm (1998) and Witt-Eickschen *et al*. (1998). (c) Data for crustal xenoliths from the Eifel (Stosch & Lugmair, 1984; Loock *et al*., 1990) and the Massif Central (Downes & Leyreloup, 1986). EAR, European Asthenospheric Reservoir (Cebriá & Wilson, 1995); LVC, Low Velocity Component (Hoernle *et al*., 1995), BSE, Bulk Silicate Earth (DePaolo & Wasserburg, 1979).

granulites also are high in $^{87}Sr/^{86}Sr$. Most xenoliths studied have both lower $^{143}Nd/^{144}Nd$ and higher $^{87}Sr/^{86}Sr$ than Vogelsberg basaltic rocks, but a few xenoliths from the Eifel and NHD overlap with Vogelsberg tholeiites. Pb isotopic compositions (Fig. 7) fall to the left of the NHRL (Hart, 1984) in both $^{206}Pb/^{204}Pb$ vs $^{207}Pb/^{204}Pb$ and $^{206}Pb/^{204}Pb$ vs $^{208}Pb/^{204}Pb$. Metasedimentary granulitic gneisses have much higher $^{87}Sr/^{86}Sr$ and lower $^{143}Nd/^{144}Nd$ than mafic granulites, but similar Pb isotopic compositions. Mafic granulites from the NHD overlap with alkali basalts from the Vogelsberg. The mineralogical and geochemical composition of some representative crustal xenoliths from the literature is given in Table 3.

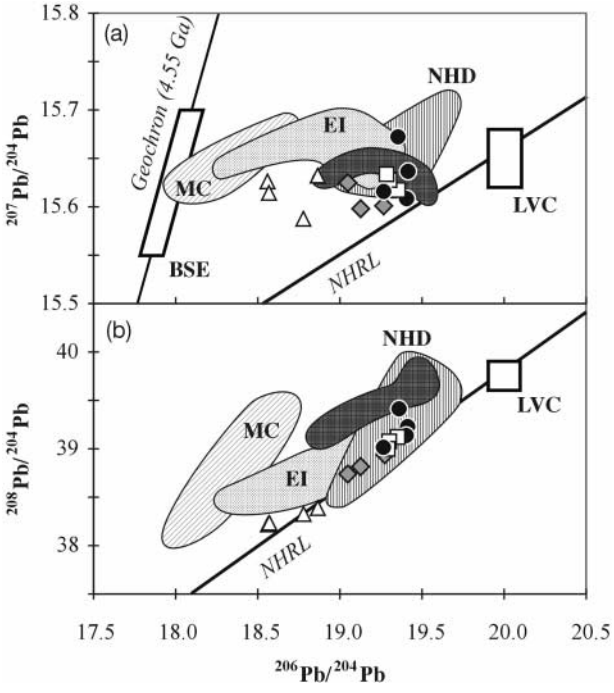

Fig. 7. (a) $^{206}Pb/^{204}Pb$ vs $^{207}Pb/^{204}Pb$ and (b) $^{208}Pb/^{204}Pb$ for basic volcanic rocks from the Vogelsberg (symbols as in Fig. 6). Bars in (a) represent analytical error (2σ). Other errors are smaller than symbol size. Grey field represents the composition of basic volcanic rocks from the Eifel (Wörner *et al*., 1986); other fields represent crustal xenoliths; EI, Eifel (Rudnick & Goldstein, 1990); MC, Massif Central (Downes *et al*., 1991). NHRL, Northern Hemisphere Reference Line (Hart, 1984); LVC, Low Velocity Component (Hoernle *et al*., 1995); BSE, Bulk Silicate Earth (Zindler & Hart, 1986).

Crustal contamination in Vogelsberg tholeiites

Vogelsberg tholeiites and alkali basalts have Sr and Nd isotopic compositions that are distinct from those of the primitive basanites. However, unlike in most major and trace element variation diagrams, in Sr vs Nd isotope space the Vogelsberg volcanic rocks do not form a continuous trend. A combination of Sr–Nd

Table 3: Representative crustal xenoliths

Sample:	S32	S35	Rp 41
Data:	Loock *et al.* (1990)	Stosch & Lugmair (1984)	Downes & Leyreloup (1986)
Type:	mafic granulite	mafic granulite	metasediment
Location:	Eifel	Eifel	Massif Central
SiO_2	52·85	47·3	62·14
TiO_2	0·45	1·95	0·18
Al_2O_3	17·76	13·6	16·66
Fe_2O_3	3·3	4·7	5·24
FeO	3·58	9·7	2·85
MnO	0·16	0·22	0·12
MgO	4·57	7·2	3·08
CaO	12·2	12·3	1·17
Na_2O	4·23	2·12	1·23
K_2O	0·25	0·22	3·51
H_2O			2·43
P_2O_5	0·31	0·27	0·05
Total	99·91		98·66
Plag	60	35	
Opx	0	10	
Cpx	33	35	
Amph	0	5	
Sph	0	0	
Gar	4	7	
M/I/S	3	5	
Mg-number	0·55	0·48	
Sc	19·4	39·5	
Cr	48	157	86
Co	20·5	47·7	22
Rb	0·94	1·25	72
Sr	1325	266·1	254
Ba			960
La	23·7	13·9	45
Ce	64	39	78·9
Nd	36·9	24·98	30·1
Sm	8·07	6·02	7·2
Eu	1·57	1·69	1·82
Gd			7·46
Yb	2·43	2·68	4·12
Lu	0·39	0·42	
Hf	3·25	2·8	
Pb	4·57	2·66	
Th	0·49	0·41	
U	0·07	0·04	
$^{87}Sr/^{86}Sr$	0·709478	0·70546	0·71876
$^{143}Nd/^{144}Nd$	0·512198	0·512343	0·512083
$^{206}Pb/^{204}Pb$	19·04	18·3	18·261
$^{207}Pb/^{204}Pb$	15·67	15·64	15·62
$^{208}Pb/^{204}Pb$	38·84	38·47	38·618

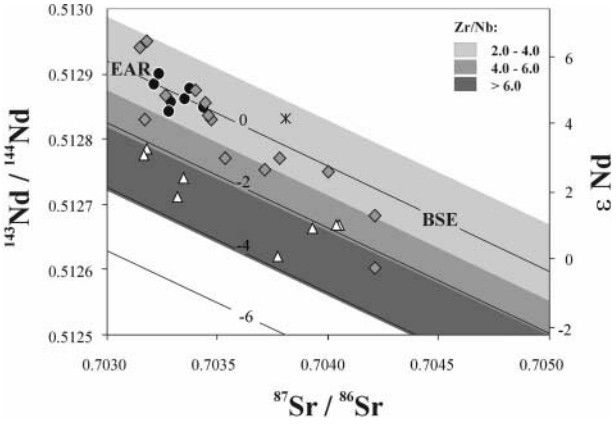

Fig. 8. $^{87}Sr/^{86}Sr$ vs $^{143}Nd/^{144}Nd$ and εNd for basic rocks from the Vogelsberg (symbols as in Fig. 6). Black lines are labelled for ΔεNd, which is defined as the vertical distance in εNd units from a line between EAR and BSE compositions (ΔεNd = 0). Grey fields represent ranges of Zr/Nb (see upper right corner of the diagram). These contours of Zr/Nb run parallel to the EAR–BSE array.

isotopes and trace element data reveals some surprising systematics. In Fig. 8, points in an $^{87}Sr/^{86}Sr$ vs $^{143}Nd/^{144}Nd$ plot are contoured for their Zr/Nb ratio. These contours are parallel to a line between EAR/LVC and BSE, where Zr/Nb increases with vertical distance from this line. In Fig. 9, the same feature is expressed in a different way: Zr/Nb is plotted against ΔεNd (Fig. 9b), which represents the vertical distance in εNd units from a line between the EAR and BSE isotopic composition:

$$\Delta\varepsilon Nd = \varepsilon Nd_{sample} - \varepsilon Nd_{EAR-BSE}$$

where

$$\varepsilon Nd_{EAR-BSE} = [(^{143}Nd/^{144}Nd_{EAR-BSE}/0{\cdot}512658) - 1] \times 10\,000$$

and

$$^{143}Nd/^{144}Nd_{EAR-BSE} = S_{EAR-BSE} \times {}^{87}Sr/^{86}Sr_{sample} + I_{EAR-BSE}$$

where $S_{EAR-BSE}$ and $I_{EAR-BSE}$ are the slope and intercept of the line between EAR and BSE compositions in Sr and Nd isotope space.

From Fig. 9 it is clear that Zr/Nb, Ce/Yb and 1/Nd correlate more strongly with ΔεNd than with $^{143}Nd/^{144}Nd$. High Zr/Nb, low Nd (or high 1/Nd) and low Ce/Yb all reflect the depleted character of tholeiites compared with basanites, and consequently the greater sensitivity to contamination processes. Therefore the observed trends may be explained by crustal contamination of the tholeiites.

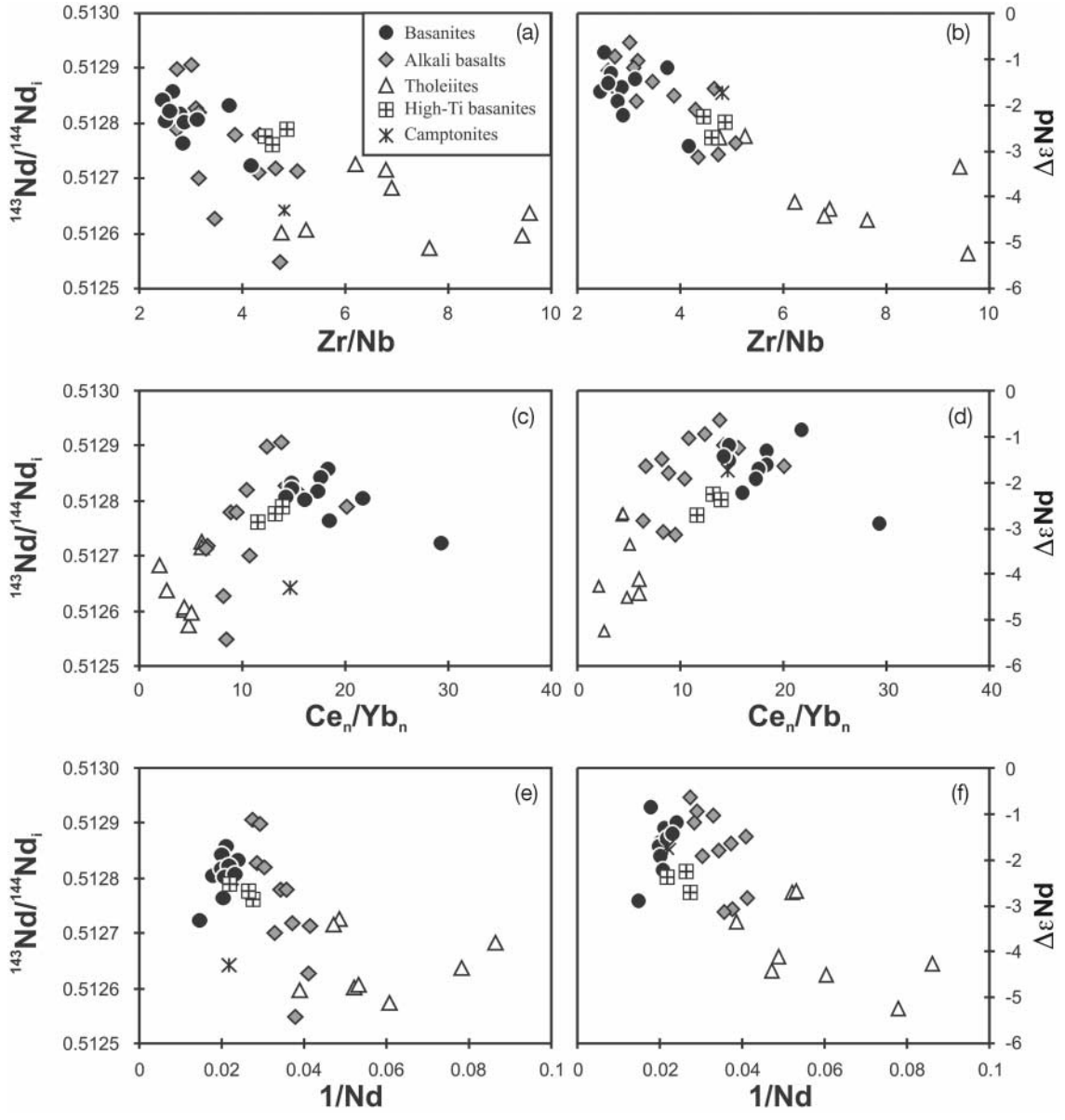

Fig. 9. $^{143}Nd/^{144}Nd$ and ΔεNd vs selected trace element ratios. (See text for calculation and explanation of ΔεNd.)

The stronger correlation of the trace element ratios with ΔεNd than with $^{143}Nd/^{144}Nd$ may be explained by assuming that before being contaminated in the crust, the tholeiites already had a range in Sr and Nd isotopic composition, broadly along a line between EAR/LVC and BSE. If the depleted tholeiite signature is derived from a mid-ocean ridge basalt (MORB)-like depleted mantle source, some uncontaminated tholeiites may even have had a more radiogenic Nd isotopic composition than the Vogelsberg basanites. Crustal contamination could then have lowered $^{143}Nd/^{144}Nd$ ratios in the contaminated magmas without significantly affecting $^{87}Sr/^{86}Sr$ ratios, displacing isotopic compositions below the line between EAR/LVC and BSE or in other words decreasing ΔεNd values.

We modelled crustal contamination of the tholeiites using the energy-constrained assimilation–fractional crystallization (EC-AFC) model of Spera & Bohrson (2001). According to the model above we used MORB-like initial Sr and Nd concentrations, and isotopic compositions varying between EAR/LVC and

Table 4: Input EC-AFC model

Thermal parameters	*T* (°C)		
Magma liquidus temperature	1280	Crystallization enthalpy	396000
Magma initial temperature	1280	Isobaric specific heat of magma	1484
Assimilant liquidus temperature	1100	Fusion enthalpy	354000
Assimilant initial temperature	900	Isobaric specific heat of assimilant	1388
Solidus temperature	950		
Equilibration temperature	980		

Compositional parameters	Sr	Nd	$^{206}Pb/^{204}Pb$	$^{207}Pb/^{204}Pb$	$^{208}Pb/^{204}Pb$
Magma A					
Magma initial concentration	115·44	5	0·42	0·42	0·42
Magma isotope ratio	0·702941	0·512958	18·5	15·5	38·25
Magma trace element distribution coefficient	0·5	0·25	0·1	0·1	0·1
Magma B					
Magma initial concentration	115·44	5	0·42	0·42	0·42
Magma isotope ratio	0·7037	0·5128129	18·5	15·5	38·25
Magma trace element distribution coefficient	0·5	0·25	0·1	0·1	0·1
*Assimilant**					
Assimilant initial concentration	266·1	24·98	2·66	2·66	2·66
Assimilant isotope ratio	0·70546	0·512343	18·3	15·64	38·47
Assimilant trace element distribution coefficient	1·5	0·35	0·25	0·25	0·25

*Composition of mafic crustal granulite S32 (Stosch & Lugmair, 1986; Table 3).

BSE ($\Delta\varepsilon Nd = 0$). Mafic granulite S32 from Stosch *et al.* (1986) was used as the contaminant (Table 3). The parameters used for the model are given in Table 4. Thermodynamic parameters were calculated from the tables given by Spera & Bohrson (2001). In comparison with the 'standard crustal case' from Spera & Bohrson (2001) we used a higher initial temperature for the continental crust. This was done to reflect heating of the crust by rifting, uplift of the asthenosphere–lithosphere boundary and sustained magmatism below the Vogelsberg. The main effect of this is that the total amount of fractional crystallization necessary to start assimilation, and therefore the enrichment of incompatible elements in the magma before contamination commences, is strongly reduced.

Figure 10 shows results of the model calculations. The systematic displacement of Sr and Nd isotope compositions below the line between EAR and BSE is obvious. The relatively low sensitivity of Sr isotopic compositions to the earliest stage of crustal contamination is caused by the presence of residual plagioclase during partial melting of lower-crustal rocks. As a result of the high partition coefficient of Sr in plagioclase, Sr is low in the contaminant crustal melt and thus Sr isotopic compositions in the magma are not significantly affected. Nd in contrast is strongly incompatible during partial melting of the crust, and even low amounts of crustal contamination have a strong effect on Nd isotopic composition.

Figure 10a shows two contamination curves. The two curves have different Sr and Nd isotope starting compositions, both with $\Delta\varepsilon Nd = 0$. This results in different trajectories in Fig. 10a, but very similar trajectories in Fig. 10b. The trend of the Vogelsberg volcanic rocks in Fig. 10b can be explained by similar amounts of contamination of variably depleted parental magmas: the most strongly depleted parent magma (lowest Nd or highest 1/Nd) is the most sensitive to crustal contamination (low $\Delta\varepsilon Nd$).

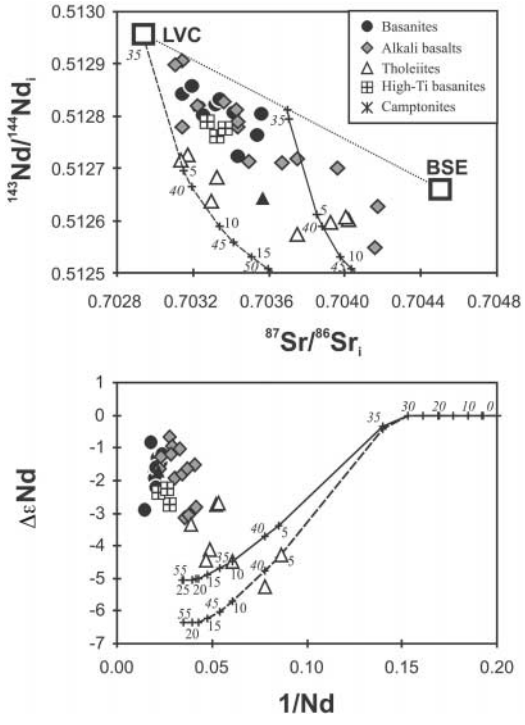

Fig. 10. Results of EC-AFC calculation. Broken and continuous lines with numbers show calculated curves for Magma A and B, respectively (Table 4). Italic numbers give the total amount of fractional crystallization; other numbers give the percentage of assimilant in the melt.

Pb isotopic compositions of tholeiites may also be strongly affected by contamination. However, the entire observed range in Pb isotopes in Vogelsberg magmas (Fig. 10c) cannot be explained by contamination alone. Some prior isotopic differences between the sources of basanites and tholeiites must be assumed. The Pb isotope compositions of tholeiites plotting along the NHRL (Hart, 1984) require the involvement of a MORB-like mantle source component. EC-AFC calculations predict very strong enrichment of Pb in the contaminated melt during the early stages of contamination because of the strong incompatibility of Pb during partial melting of the crust. Such enrichment is not observed in the Vogelsberg tholeiites. Possible explanations for this discrepancy are that (1) Pb is retained by some accessory phase during partial melting of lower-crustal rocks or (2) Pb concentrations are very low in the crustal contaminant. No crustal xenolith data from the Vogelsberg region itself are available. Available crustal xenolith data from surrounding regions (Table 3 and references) show wide variations in mineralogy and Pb contents. Therefore no robust conclusions can be drawn on the influence of crustal contamination on Pb isotope compositions of Vogelsberg tholeiites.

MANTLE SOURCE SIGNATURES

Basanites and primitive alkali basalts: EAR mantle signature

The Vogelsberg primary basanites and primitive alkali basalts have Sr, Nd and Pb isotopic compositions close to the EAR/LVC (Cebriá & Wilson, 1995; Hoernle *et al.*, 1995) end-member composition of Central European Tertiary volcanic rocks (Figs 6 and 7). The incompatible trace element concentrations of basanites and primitive alkali basalts closely match those of other primitive mafic volcanic rocks from the Tertiary CEVP (Wilson & Downes, 1991). Altogether, these features suggest that Vogelsberg basanites and alkali basalts derive from variable degrees of partial melting of a source located in the convecting asthenosphere (Wilson & Downes, 1991).

To better constrain this source, we performed inverse trace element model calculations based on the observed trace element compositions of the primitive basanites and alkali basalts. The approach is as follows: slopes and intercepts in plots of C^i vs C^i/C^j, where C^i and C^j are the concentrations of a very incompatible element i and a less incompatible element j in samples related by variable degrees of partial melting of a similar source, allow us to infer the trace element composition and source–liquid partition coefficients of the mantle source (Allègre *et al.*, 1977). Minster & Allègre (1978) developed the inverse modelling method, which was later simplified by Hofmann & Feigenson (1983), Ormerod *et al.* (1988) and Cebriá & López-Ruiz (1996). The calculations given here follow the model of Cebriá & López-Ruiz (1996). The major advantage of their model is that it does not make any assumptions about melting mode or partition coefficients of the melt mode (P_L). Rather, the model is constrained by assuming that the range of Yb and Lu concentrations in typical mantle peridotites is limited to between two and four times chondritic values (Frey, 1984; McDonough & Frey, 1989). This assumption allows the independent determination of three parameters. First, it is possible to establish ranges of P_L values for Yb and Lu for a range of melting degree (F). Second, it allows determination of ranges of source concentration values (C_0^i) for highly incompatible elements for any given $P^{Yb,Lu}$ and F. Third, it gives possible ranges of F. These constraints are then used to obtain a best fit for the degree of melting F and for the source concentration (C_0^i), bulk distribution coefficient (D_0^i), and P_L^i) for selected elements using iterative methods. These values can be used to further constrain C_0, D_0 and P_L values for the remaining elements.

For a range of samples to be related by variable degrees of melting of a common homogeneous mantle source, the samples should plot on straight lines in plots

Table 5: Parameters and results of inverse batch melt modelling (see text for discussion)

	R	Slope	Intercept	D_0	P_L	C_0	C_0/Primitive Mantle
Ba	0·64	0·65	0·47	0·050	0·214	67·53	10·91
Th	0·91	0·14	0·09	0·008	0·019	0·36	4·21
U	0·83	0·27	0·17	0·014	0·098	0·09	4·21
Nb	0·77	0·35	0·22	0·018	0·128	4·09	6·29
La	0·83	0·15	0·13	0·008	0·032	3·00	4·81
Ce	0·85	0·17	0·14	0·010	0·074	5·92	3·62
Pr	0·84	0·17	0·13	0·009	0·071	0·61	2·55
P	1·00	0·00	0·00	0·0014	0·0221	140·00	1·47
Nd	0·87	0·19	0·15	0·010	0·082	2·49	2·03
Sm	0·78	0·45	0·35	0·028	0·174	0·62	1·63
Gd	0·89	0·58	0·44	0·04	0·21	0·56	1·07
Dy	0·66	0·79	0·70	0·12	0·25	0·79	1·22
Y	0·32	0·86	0·68	0·13	0·26	4·40	1·09
Er	0·38	0·89	0·75	0·18	0·28	0·51	1·20
Yb	0·14	0·98	0·76	0·23	0·37	0·50	1·14
Lu	0·07	1·03	0·77	0·31	0·40	0·10	1·48

of C^i vs C^i/C^j. This holds true for samples from Stage III of the FBV (VB96-01 to VB96-26, where P_2O_5 was used as highly incompatible element C^i), with the exception of samples VB96-01, -10 and -19. Samples VB96-01 and VB96-19 have high Mg-number and show petrographic evidence of olivine accumulation. Sample VB96-10 has anomalous concentrations of several trace elements (e.g. Ba) and may have been contaminated. Correlation coefficients for trace elements used in the model are given in Table 5 together with slopes in plots of P_2O_5 vs P_2O_5/C^j and intercepts in plots of P_2O_5 vs C^j. The latter are plotted in Fig. 11. This plot was used by Cebriá & López-Ruiz (1996) to infer the order of incompatibility of the elements used for inverse modelling.

In the model example given by Cebriá & López-Ruiz (1996), F is well constrained by the assumption that Yb and Lu concentrations in the mantle source vary between two and four times the chondritic concentration. This does not hold true here: any degree of melting between 3 and 50% can produce the required concentrations for our model. Therefore we used an external constraint on the degree of melting based on major element composition. Chen (1988) calculated degrees of melting for a range of rock types from the Northern Hessian Depression that are similar to the Vogelsberg rocks based on $Na_2O + K_2O$ contents and Al_2O_3/SiO_2 ratios of melts and estimated mantle sources. He obtained 4·9–6·4% melting for nephelinites, 7·3–8·7% for alkali basalts, and 11·3% for an olivine tholeiite. From these estimates it can be deduced that the degree of melting for primitive alkali basalts (46 wt % SiO_2), which represent the highest degree melts in our calculation, is unlikely to exceed 10%. We used 7·3% as an input value for the iteration, and F_{max} was allowed to vary between 5 and 10%.

Results of the model calculation are given in Table 5. The general shape of the obtained source concentration pattern C_0 (Fig. 11b) is in good agreement with results from Cebriá & López-Ruiz (1996) for similar rocks from Calatrava, Spain, that are also inferred to be EAR related. However, absolute concentrations of highly incompatible elements are lower by as much as a factor of two in our calculations. This discrepancy may be ascribed to a large difference in the inferred maximum degree of melting. Cebriá & López-Ruiz (1996) derived degrees of melting entirely from the melting model. As shown above, the degrees of melting given here are externally constrained.

The calculations indicate a more moderate enrichment of highly incompatible elements over Yb and Lu—by a factor of four less for La—compared with the findings of Cebriá & López-Ruiz (1996). Depletion of Th and U relative to Ba and Nb, which is observed for all Vogelsberg rocks, is reproduced as a primary feature of the mantle source. Calculated D_0 values strongly decrease from Yb–Lu to Nd and then show broadly similar values for Pr–Th, which is consistent with similar slopes and intercepts in C^i vs C^i/C^j diagrams for these elements. D_0^{Ba} is distinctly higher and D_0^{P} distinctly lower than D_0 for neighbouring elements. Values of P_L broadly parallel D_0, but are almost

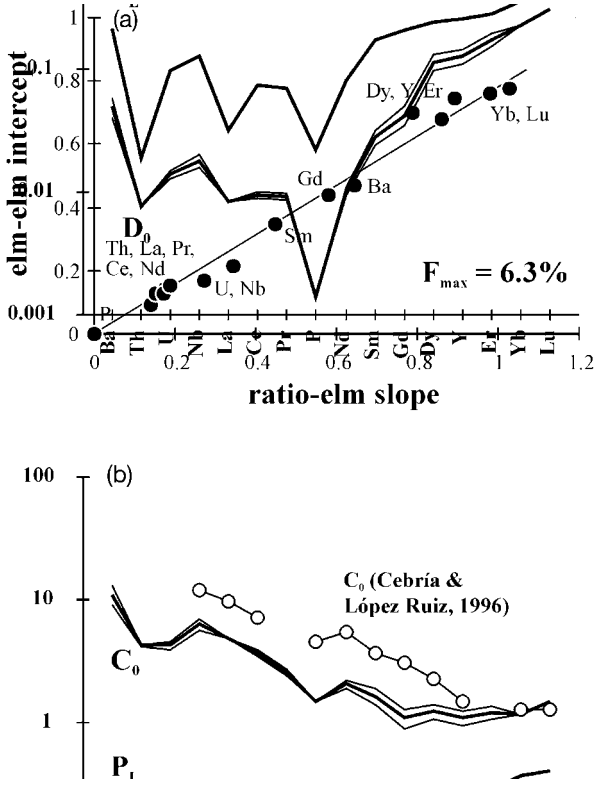

Fig. 11. (a) Slopes of P_2O_5 vs P_2O_5/C_L^i (ratio–elm slope) plotted against intercepts of P_2O_5 vs C_L^i (elm–elm intercept; see text for discussion); (b) modelled C_0, D_0 and P_L (bold lines) for the source of EAR-type melts (see text for discussion). Fine lines give upper and lower limits of C_0 and D_0. Curve with circles gives the EAR composition as calculated by Cebriá & López-Ruiz (1996). F_{max} is the degree of melting needed to produce the composition of sample VB-16, which is the sample with lowest trace element concentration used in the calculation.

an order of magnitude higher for most elements. P_L^{La} and P_L^{Th} show much stronger negative peaks in the P_L curve than in the D_0 curve.

The model gives clues about the mineralogy of the source as well as the amount of phases contributing to the melt. Our calculated values for $D_0^{Yb,Lu}$ and $P_L^{Yb,Lu}$ are similar to clinopyroxene–liquid partition coefficients usually reported in the literature (e.g. McKenzie & O'Nions, 1991; Zack *et al.*, 1997, and references therein). On the other hand, Blundy *et al.* (1998) showed that partition coefficients for heavy rare earth elements (HREE) in clinopyroxene may be much higher close to the solidus of spinel lherzolite. High Mg-number and Ni and Cr concentrations require an olivine-bearing peridotitic source for the basanites, rather than a pyroxenite source. The obtained partition coefficients for Yb and Lu therefore indicate low degrees of partial melting in a spinel lherzolite source, or the presence of residual garnet. Assuming a peridotitic source, published garnet–liquid partition coefficients (McKenzie & O'Nions, 1991; Zack *et al.*, 1997) suggest a maximum garnet contribution of 5% in the source and 8% in the melt. Forward calculated melt compositions based on a garnet-bearing and a spinel peridotite source are depicted in Fig. 12. The melting curve of our inverse model lies between batch melting curves for garnet and spinel peridotite.

Vogelsberg basanite trace element patterns (Fig. 5a) show large negative K anomalies and highly variable Rb concentrations. Neither K nor Rb correlates with P or La/Yb. Such depletion of K and Rb may be a primary feature of mantle plume sources (Thirlwall *et al.*, 1994). However, these elements are also likely to be affected to some extent by surface weathering (Bogaard *et al.*, 2001*a*). None the less, many workers (e.g. Wilson & Downes, 1991; Cebriá & Wilson, 1996; Jung & Masberg, 1998) have attributed the K depletion to a residual K-bearing phase (e.g. amphibole, phlogopite) in the mantle source. This may be evaluated by considering partition coefficients for Ba. D_0^{Ba} and P_L^{Ba} are moderately high (0·05 and 0·2, respectively) in our model, even though typical peridotite minerals (olivine, orthopyroxene, clinopyroxene, garnet, spinel) all have very low Ba partition coefficients. Mantle amphiboles and phlogopites have D^{Ba} of 0·1–1 (Brenan *et al.*, 1995; Ionov & Hofmann, 1995; LaTourette *et al.*, 1995; Zack *et al.*, 1997) and 3·7–10 (Villemant *et al.*, 1981; LaTourette *et al.*, 1995), respectively. Thus, the observed Ba contents of the magmas could be explained by small amounts of phlogopite and/or larger amounts of amphibole in the source of the basanites.

Although the inverse model may give a good approximation of source concentrations, partition coefficients and range of F needed to produce the Vogelsberg basanites, it also has limitations. The most obvious is that batch melting, although a good first approximation, is not the real process by which decompression melts are formed. Rather, melting is likely to be near fractional (Johnson *et al.*, 1990) and polybaric (Klein & Langmuir, 1989). Such models allow a different interpretation on the role of garnet during

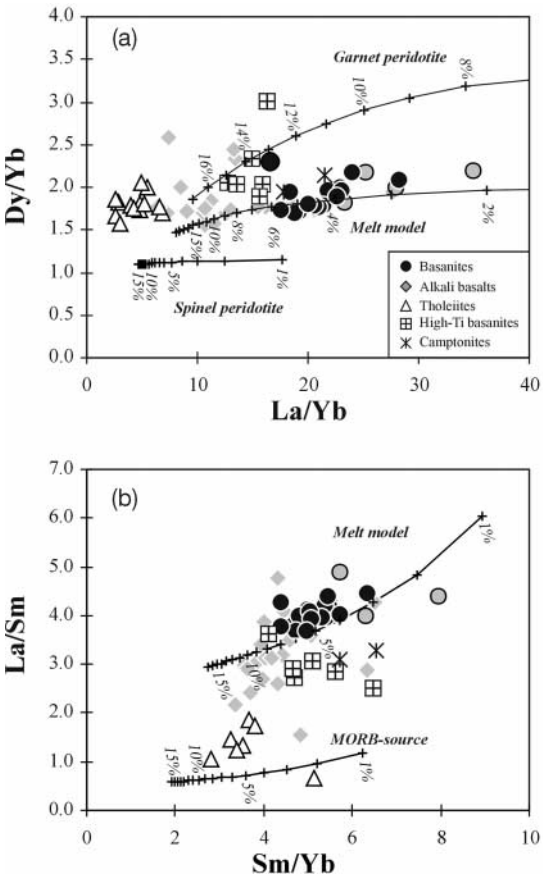

Fig. 12. (a) La/Yb vs Dy/Yb for basic volcanic rocks from the Vogelsberg. Also shown are melt curves for garnet peridotite, spinel peridotite and the inverse batch melting model (see text). The position of melt model curve between garnet and spinel curves should be noted. (b) Sm/Yb vs La/Sm, plus melt curves for the inverse batch melting model and a curve with the same parameters except for a depleted (MORB) source composition. The figure demonstrates that tholeiites, apart from somewhat higher degrees of melting, also require a more depleted source composition than basanites and alkali basalts.

melting. Seismic models show that the asthenosphere–lithosphere boundary beneath the Vogelsberg is strongly elevated, in response to rifting and mantle upwelling, to depths of 50–70 km (Babuska & Plomerova, 1992). The garnet to spinel transition takes place at pressures of 3–2·5 GPa (McKenzie & Bickle, 1988). Therefore, melting probably takes place for a considerable part in the garnet–spinel transition zone.

In Fig. 12a, La/Yb is plotted against Dy/Yb for the Vogelsberg mafic volcanic rocks. This plot was used by Thirlwall *et al*. (1994) to distinguish between melting of garnet and spinel peridotite. Because Yb is compatible in garnet, whereas La is strongly incompatible, La/Yb ratios will be extremely fractionated during the early stages of melting in the garnet stability field. Dy/Yb is also fractionated in the presence of residual garnet, but this effect is also seen for higher degrees of melting. Melting in the garnet stability field therefore produces strongly curved arrays in a Dy/Yb vs La/Yb diagram (Fig. 12a). In the spinel field, La/Yb is only slightly fractionated for small degrees of melting, and Dy/Yb is not fractionated at all. Thirlwall *et al*. (1994) argued that melts from the garnet–spinel transition zone would have characteristics almost identical to garnet-facies melts, until garnet was exhausted during melting. On average, however, melts from the garnet–spinel transition zone will have lower proportions of garnet in the source. The fractionation of REE should therefore be less pronounced. Vogelsberg basanites lie between model curves for garnet peridotite and spinel peridotite in Fig. 12a. This is interpreted as indicating that melting of the EAR-reservoir took place in the garnet–spinel transition zone.

La/Sm–Sm/Yb relations (Fig. 12b) are also sensitive to the presence of garnet or spinel in the source, but give more important clues about enrichment vs depletion of the mantle source. Whereas basanites straddle the model melting curve, tholeiites and alkali basalts clearly require that their source was trace element depleted. The tholeiites have slightly higher La/Sm ratios than the average N-MORB from Sun & McDonough (1989), but much higher Sm/Yb and Dy/Yb ratios. As shown in Fig. 12b, these features cannot be explained by mixing of basanitic melts with N-MORB. Rather, Vogelsberg tholeiites are probably smaller-degree melts from greater depth than average N-MORB, but still derived from a depleted source.

Tholeiites and evolved alkali basalts: interaction of depleted mantle melts with metasomatized sub-continental lithospheric mantle?

On the basis of the preceding discussion several important points can be made concerning the formation of the Vogelsberg tholeiites and alkali basalts: (1) whereas basanites formed by small degrees of partial melting of an EAR-type source, the tholeiites and evolved alkali basalts require the additional involvement of a (relatively) trace element depleted mantle source component; (2) tholeiite Sr- and Nd-isotopic compositions below the mantle array may be explained by crustal contamination; (3) before crustal contamination, tholeiites may have had Sr- and Nd-isotopic compositions between EAR/LVC and BSE, similar to evolved alkali basalts. A similar range of isotopic variation is observed in other regions of the CEVP and also in many metasomatized mantle xenoliths from the

SCLM from those areas. This observation has led to the idea that the basalt isotopic compositions result from interaction between asthenospheric melts with metasomatized SCLM (e.g. Wilson & Downes, 1991; Cebriá & Wilson, 1995; Hoernle *et al*., 1995). The exact nature of this interaction is, however, as yet unknown.

The possible role of metasomatized lithospheric mantle in the origin of the Vogelsberg tholeiitic and alkali basaltic magmas may be inferred from the study of mantle xenoliths from the CEVP. Detailed surveys of xenolith suites from the Eifel (Rosenbaum & Wilson 1996; Witt-Eickschen & Kramm, 1998; Witt-Eickschen *et al*., 1998) have revealed the presence of at least two metasomatic episodes. An old metasomatic event produced very strong enrichment of light REE (LREE) and large ion lithophile elements (LILE) but not of HFSE. Sr- and Nd-isotope compositions of xenoliths with these signatures fall below the EAR–BSE array of the volcanic rocks (Fig. 6a). Metasomatically enriched xenoliths from the Rhön have similar trace element characteristics (Witt-Eickschen & Kramm, 1997). This event is attributed to modification of depleted mantle by fluids released from subducted oceanic crust during the Hercynian orogeny (Wörner *et al*., 1986; Kempton *et al*., 1988; Rosenbaum & Wilson, 1996), which may have resulted in enrichment of LILE over HFSE. Rocks with this signature, however, cannot represent a source component for the volcanic rocks (Stosch & Lugmair, 1986).

A second metasomatic event is found in the form of composite xenoliths. Isotopic and trace element compositions of the veins in these xenoliths overlap with that of the lavas (Fig. 6a). However, the preservation of trace element variations within minerals in contact aureoles around the veins in some of these xenoliths shows that formation of these veins and metasomatic overprint of the surrounding host-rock cannot have happened more than $\sim$1000 years before the xenoliths were transported to the surface (Witt-Eickschen *et al*., 1998). Also, geochemical characteristics suggest that the metasomatic overprint resulted from infiltration of melts similar to the Eifel volcanic rocks (Witt-Eickschen & Kramm, 1998; Witt-Eickschen *et al*., 1998). If this interpretation is correct, the compositional range of veins simply mirrors the composition of the volcanic rocks, but cannot explain them. In that case, no potential SCLM source component is represented by the mantle xenoliths.

A possible way out of this dilemma could be that a metasomatic event that produced BSE-like isotope signatures did precede the Tertiary volcanism by a long time, but that heating of the SCLM by EAR melts remobilized the metasomatized portions of the mantle, thereby giving the impression that the metasomatic event itself was in fact young. Evidence for a vertical variation in metasomatic style in the mantle is preserved in the Dreiser Weiher xenolith suite from the Eifel. Low-temperature metasomatized xenoliths [1a suite of Stosch & Seck (1980)] are hydrous, and metasomatism resulted in the formation of amphibole and phlogopite. In contrast, high-temperature and presumably deeper xenoliths [1b suite of Stosch & Seck (1980)] do show evidence of metasomatic enrichment, but are anhydrous.

Unfortunately, for the Vogelsberg and closely related Northern Hessian Depression, no xenolith data of the type as for the Eifel and Rhön are available. Although overall Sr, Nd and Pb isotopic variations for these regions are similar, the rock types displaying especially the BSE-like signatures are very different. In the Eifel, these signatures are found in highly enriched potassic rocks (Wörner *et al*., 1986), whereas in the Vogelsberg they are found in alkali basalts and tholeiites that are relatively depleted in incompatible trace elements compared with EAR-related basanites. Clearly, more detailed xenolith data from the Vogelsberg and Northern Hessian Depression are necessary to explain these differences.

High-Ti basanites: melts of hydrous mineral-bearing veins

High-Ti basanites are distinct in terms of their major (MgO, Al_2O_3, TiO_2) and trace element characteristics (Zr/Nb, LREE, Ba/Zr) from normal basanites. It was suggested previously that the low Mg-number of the high-Ti basanites is not easily explained by fractional crystallization of primary basanitic magmas, but may rather reflect the involvement of significant amounts of hydrous minerals in their source. A special case of such a process is the melting of hydrous mineral bearing veins in a peridotitic or harzburgitic matrix (Foley, 1992). Such veins may form in lowermost lithosphere as a result of infiltration of very small degree asthenospheric mantle melts, at the transition zone between porous flow and dyke-flow regions. Hydrous mineral assemblages have lower melting points than normal mantle peridotite. Therefore, upon heating or uplift of the asthenosphere–lithosphere boundary, these veins will be the first to melt (Hawkesworth & Gallagher, 1993). No direct evidence for such veins, in the form of composite xenoliths, has been found in the Vogelsberg area. Such evidence is, however, preserved in the form of distinct Fe–Ti enrichment in some high-T mantle xenoliths (Witt-Eickschen, 1993). Most mantle xenoliths in the Vogelsberg area are found in 'normal' basanites, which erupted $\sim$2 Myr after the high-Ti basanites. Partial melting of veins during lithospheric stretching could have 'melted out' the veined lithospheric source of the high-Ti basanites by the time

Table 6: Experimental vein melt compositions compared with high-Ti basanite and camptonite compositions

	Experimental vein melt compositions					high-Ti basanites			camptonite
Mineral:	N1	N2	N3	N4	N5	VB96-92	VB98-135	VB98-145	11315
Assemblage:	50Am	45Am	45Am	40Am	50Cpx				
	50Ap	45Ap	45Ap	40Ap	50Mica				
		10Cpx	10Mica	10Cpx					
				10Mica					
SiO_2	36·76	37·64	38·73	37·30	39·46	45·41	44·24	43·21	44·99
TiO_2	6·18	5·39	5·17	6·06	3·62	3·52	4·22	4·38	3·88
Al_2O_3	13·04	13·18	14·16	15·66	13·32	13·19	14·78	13·95	15·29
FeO*	12·77	12·63	12·41	10·33	20·37	12·28	11·43	13·75	12·02
MnO						0·19	0·17	0·18	0·19
MgO	9·59	7·43	6·54	13·95	8·45	8·19	6·90	8·61	5·73
CaO	14·56	15·19	14·71	6·94	6·31	12·02	12·75	10·84	11·18
Na_2O	2·76	2·69	1·90	2·15	0·80	2·52	3·44	3·06	2·54
K_2O	1·83	1·89	2·95	5·06	6·52	1·09	0·94	0·93	2·62
P_2O_5	1·78	3·25	2·91	2·05	1·09	0·60	0·52	0·62	1·13
Total	99·27	99·29	99·48	99·50	99·94	100·00	100·00	100·00	100·00
Mg-no.	64·0	58·2	55·5	76·2	49·6	58·3	55·9	56·8	1·03
K_2O/Na_2O	0·66	0·70	1·55	2·35	8·15	0·43	0·27	0·30	50·0

Vein compositions are non-cratonic assemblages from Foley *et al.* (1999). (See text for discussion.)

that the normal basanites formed. High-Ti basanites are the earliest mafic volcanic rocks erupted in the Vogelsberg area. Hornblende basalts from the Rhön with similar geochemical characteristics also formed the earliest mafic melts of that area (Ehrenberg & Hickethier, 1994).

Foley *et al.* (1999) performed melting experiments on 'vein assemblages' rich in amphibole, mica, apatite and clinopyroxene. The compositions of their experimental melts are compared in Table 6 with the whole-rock compositions of the high-Ti basanites and a camptonite. The experimental melts all have low SiO_2, MgO and Mg-number and high TiO_2, similar to our high-Ti basanites. Melts from the mica-bearing assemblages are potassic and have low calcium contents, which are not observed in the high-Ti basanites. The presence of apatite results in high phosphorus contents in the vein melts. All experimental 'vein' assemblages in Table 6 have 50 vol. % or more hydrous minerals. However, Witt-Eickschen (1993) has argued that Ti enrichment in mantle xenoliths from the Vogelsberg formed in contact aureoles around pyroxenitic veins. It is therefore proposed here that high-Ti basanites represent melts of veins rich in pyroxene with limited amphibole, explaining the more basaltic compositions compared with experimental melts described by Foley *et al.* (1999). Evidence for the presence of residual amphibole during melting of these veins is given by negative K anomalies in the trace element patterns of high-Ti basalts. Furthermore, both high-Ti basanites and hornblende basalts from the Vogelsberg and Rhön often carry amphibole phenocrysts.

Late Cretaceous camptonitic dykes from the Vogelsberg area have trace element characteristics (e.g. Zr/Nb and Ti/Zr) similar to the high-Ti basanites. Their age suggests that their formation may have been related to the initial upwarping of the 'Rhenish Dome', which includes the Rhenish Shield, parts of the Northern Hessian Depression, the Black Forest and the Vosges Mountains (Becker, 1993). During this period, amphibole–pyroxene-rich veins could have formed in the lower lithosphere of the area. Camptonites could then represent the surface expression of this event.

High-Ti basanites have a relatively large variation in their Sm/Yb ratios, and fall on a trend opposite to the melting curves in Fig. 12b. This could reflect mixing between vein melts and melts from surrounding host peridotite, as predicted by Foley (1992). The high Sm/Yb, low La/Sm end of this trend would then represent the vein-melt, as shown by the composition of camptonites.

Although absolute trace element concentrations and some trace element ratios of the high-Ti basanites are significantly different from those in normal basanites, overall trace element patterns and Sr-, Nd- and Pb-isotopic compositions are similar for the two rock types. This suggests that melts that formed the veined source for the high-Ti basanites were themselves derived from a mantle source similar to the EAR. This is consistent with interpretations that the EAR source was present and active since at least 60 Ma below Central Europe (Wilson & Patterson, 2002). Slight differences in the isotopic composition of the two rock types are then explained by isotopic evolution in the veins since their formation ~70 Myr ago.

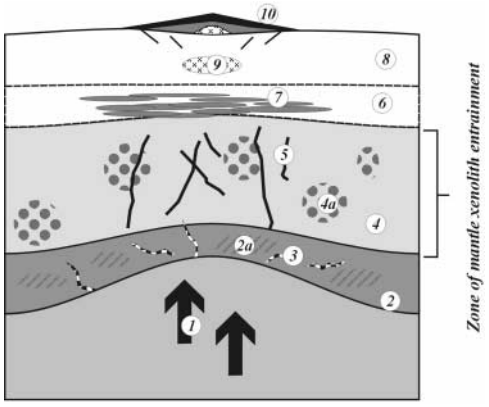

Fig. 13. Schematic representation of important components of the upper mantle and crust beneath the Vogelsberg. The earliest melts are formed in the veined lithospheric mantle source. These melts, with Zr/Nb ratios of ~4·0, are gathered in a crustal magma chamber (dotted line), where hawaiites to trachytes are formed by fractional crystallization. In a second stage, a depleted mantle source (DMS) with high Zr/Nb, located in the uppermost asthenosphere or lower lithospheric mantle, melts to form tholeiites and alkali basalts. The latter are mixtures of DMS melts with melts from upwelling asthenospheric mantle. Tholeiites and alkali basalts interact with metasomatized regions from the sub-continental lithospheric mantle (broken line), where they acquire a range of isotopic compositions between European Asthenospheric Reservoir and Bulk Silicate Earth compositions. Some of these melts may intrude at the crust–mantle boundary. In this region, crustal contamination of tholeiites takes place, which results in a decrease of $^{143}Nd/^{144}Nd$, whereas Sr isotopes are unaffected. In the last stage, melts from the upwelling asthenosphere with EAR signature rapidly rise to the surface, without significant interaction with the SCLM or the crust. 1, Upwelling asthenosphere (EAR signature); 2, lower lithospheric mantle (depleted); 2a, metasomatized regions of the TBL (anhydrous); 3, hydrous mineral bearing veins (~70 Ma?); 4, upper lithospheric mantle (depleted); 4a, metasomatized regions of the MBL (Hercynian, hydrous); 5, veins related to Tertiary volcanism; 6, lower crust; 7, Tertiary intrusions (alkalic and/or tholeiitic); 8, middle and upper crust; 9, magma chamber (alkaline differentiates); 10, Vogelsberg.

SUMMARY AND CONLUSIONS

Source characteristics of Vogelsberg magmas

At least three mantle sources are inferred for the petrogenesis of Vogelsberg basaltic rocks (Fig. 13): (1) an asthenospheric OIB-type intra-plate source akin to the EAR/LVC for the basanites and alkali basalts; (2) a relatively depleted mantle source (DMS) for the tholeiites; (3) a veined lithospheric mantle source (VLM) for the high-Ti basanites.

Basanites and primitive alkali basalts are dominated by the EAR/LVC source. Their similarity to OIB and other primitive mafic rocks from Central Europe supports the conclusion that this component is located in the convecting asthenosphere (Wilson & Downes, 1991; Fig. 13). Trace element signatures of these rocks are consistent with variable degrees of partial melting in a source that contains limited amounts of garnet and a K-bearing phase (amphibole or phlogopite). The small amount of garnet inferred can also be explained by melting (partly) within the garnet–spinel transition zone. Seismic data show that the asthenosphere–lithosphere boundary today lies at ~70 km depth below the Vogelsberg region, which is consistent with the inferred asthenospheric nature of the basanite source.

Many workers have argued that mantle plumes must be involved in the generation of CEVP volcanic rocks. For the small amounts of lithospheric stretching observed in continental rift zones such as the CEVP (Merle *et al.*, 1998), melting of the convecting asthenosphere requires anomalously hot upper mantle (McKenzie & Bickle, 1988; Wilson & Downes, 1991). Evidence for the presence of anomalously hot mantle is given by the observation that lithospheric extension in the CEVP is associated with uplift rather than subsidence (White & McKenzie, 1989; Wilson & Downes, 1991). Raikes & Bonjer (1983), Granet *et al.* (1995) and Ritter *et al.* (2001) demonstrated the existence of zones of low seismic velocity extending to 400 km depth in the mantle beneath the Quaternary Eifel and Massif Central volcanic areas. Geochemical evidence for the involvement of mantle plumes includes the overall similarity in trace element composition between CEVP volcanic rocks and OIB (Wilson & Downes, 1991), Sr, Nd and Pb isotope compositions similar to HIMU-OIB (Hoernle *et al.*, 1995; Wilson & Downes, 1991), and characteristic OIB-type trace element ratios such as high Ce/Pb (Chauvel *et al.*, 1992). It is still controversial as to whether this signature is derived from a large, deep mantle plume (Hoernle *et al.*, 1995; Goes *et al.*, 1999; Wedepohl & Baumann, 1999), or from several small plumes or diapirs from a common, relatively shallow asthenospheric reservoir (Wilson & Patterson, 2002).

REE systematics (Fig. 12) show that the depleted mantle source (DMS) component is most strongly represented in the tholeiites, but also contributes to

most alkali basalts. The DMS component is similar in composition to depleted MORB mantle. Tholeiites and alkali basalts represent higher average degree melts from shallower average depth than basanites. Therefore, it can be inferred that the depleted source must be located at shallower depths than the EAR source (Fig. 13). Stosch & Lugmair (1986) showed that there is an inverse relationship between major element fertility and trace element enrichment in peridotite xenoliths from the Eifel region. Thus, if the melting of anhydrous, deep lithosphere takes place below the Vogelsberg region, the resulting melts are most likely to have a depleted trace element composition. On the other hand, if entrainment of asthenosphere surrounding a rising plume head occurred, thermal modelling indicates that this probably happened at the centre of the rising plume (Farnetani & Richards, 1995). However, from geophysical data (Granet *et al.*, 1995; Ritter *et al.*, 2001) there is no evidence for a large-scale plume head. Depleted melts from the Vogelsberg region are affected by fractional crystallization, crustal contamination, and contamination by metasomatized lithospheric mantle. Therefore no further conclusion can be drawn about the origin and location of the depleted source component.

Source metasomatism and contamination

Many alkali basalts and tholeiites with relatively depleted trace element signatures have radiogenic Sr-isotope compositions. These signatures are derived either from interaction of DMS- and EAR-derived melts with metasomatized sub-continental lithospheric mantle, or from metasomatic overprint of previously depleted rocks within the DMS itself (Hartmann & Wedepohl, 1990). This produced a range of Sr-, Nd- and Pb-isotopic compositions between EAR and Bulk Silicate Earth (BSE) in the Vogelsberg volcanic rocks. Mantle xenoliths from Quaternary volcanic rocks from the Eifel show evidence of at least two metasomatic episodes (Hartmann & Wedepohl, 1990; Witt-Eickschen & Kramm, 1998; Witt-Eickschen *et al.*, 1998; Fig. 13). Geochemical characteristics of the older of these events do not match the associated volcanic rocks. Evidence is preserved that the youngest of these events, whose characteristics do match the volcanic rocks, is closely related in time to the Quaternary volcanism. Therefore, this event mirrors the isotopic compositions of the volcanic rocks, rather than explaining them. It is proposed here that a metasomatic event with BSE-like isotope characteristics preceded Neogene volcanism by a significant amount if time (i.e. tens of millions of years), but that heating of the SCLM by intruding lavas remobilized previously metasomatized sections into the erupted alkali basalt magmas.

After acquiring a range in Sr-, Nd- and Pb-isotopic compositions, tholeiites and evolved alkali basalts were further contaminated in the lower continental crust (Fig. 13). This resulted in a decrease in $^{143}Nd/^{144}Nd$. Deviations in Nd isotopic compositions from the EAR-BSE array are inversely correlated with Zr/Nb and 1/Nd. These correlations do not directly result from crustal contamination, but rather reflect that the most depleted melts are the most sensitive to crustal contamination.

Evolution of mantle sources through time

High-Ti basanites form the earliest melts in the Vogelsberg area. This timing and the similarity in major element composition of these melts to experimental melts of synthetic vein assemblages are consistent with an early origin from (still) veined lithospheric mantle (VLM; Fig. 13). Evidence for the presence of veins in the SCLM beneath the Vogelsberg region is preserved in Ti–Fe enrichment style metasomatism in high-T mantle xenoliths (Witt-Eickschen, 1993). The broad similarity in trace element and isotopic compositions to EAR melts suggests that the formation of these veins is related to the EAR source. Similarities to late Cretaceous camptonitic dykes from the Vogelsberg area suggest that the formation of a veined zone may have been related to the start of uplift of the 'Rhenish Dome', $\sim$70 Myr ago.

Gallagher & Hawkesworth (1992) and Hawkesworth & Gallagher (1993) predicted a sequential evolution for basaltic volcanism involving anomalously hot mantle below rifting lithosphere. This model involved (1) derivation of the earliest melts from metasomatic veins that formed as a result of freezing of low-degree melts from the uprising plume in the lower part of the mechanical boundary layer; (2) formation of silica-saturated melts from major element depleted material from the lower SCLM, and (3) gradual domination of basalt signatures by plume-derived melts as lithospheric thinning proceeds. The evolution of melting in the Vogelsberg source region appears to have closely followed this sequence. Palaeomagnetic data from the Forschungsbohrung Vogelsberg '96 borehole reveal three distinct episodes in the evolution of the Vogelsberg, separated by magmatically quiet periods (Bogaard *et al.*, 2001*b*). During the first episode, melts similar to high-Ti basanites were pooled in mid-crustal magma chambers, where they differentiated to form hawaiites to trachytes. High-Ti basanites have major and trace element characteristics that may be explained by partial melting of metasomatic veins in the lowermost lithosphere, but trace element patterns

and isotopic compositions very similar to those of the asthenospheric signature of normal basanites. After eruption of the last trachytic sequence, the geochemical character changed abruptly to tholeiites and alkali basalts. The tholeiites are silica saturated and derived from a depleted mantle source that may be located either in the lowermost lithosphere or in the uppermost asthenosphere. Up-section, the influence of a plume-type source with EAR/LVC signature increases, until during the last episode pure EAR/LVC melts (basanites) are formed.

Sampling a well-dated drill-core section, as in this study, allows the evidence for variable sources for the Vogelsberg volcanism to be placed into a temporal scheme. The entire evolution of the Vogelsberg source region took place in a period of 2–4 Myr, and tapping of different source regions was highly episodic. Melting of the VLM source may have started as early as the Aquitanian (Ehrenberg *et al*., 1981), and lasted at most until ~16·7 Myr ago when the trachyte sequence erupted. Melting of the VLM may have stopped earlier, as the evolution of the Stage I differentiates must have taken some time. VLM melts were abruptly replaced by tholeiitic and alkali basaltic lavas from the DLM source at ~16·6 Ma. Ar–Ar dating suggests that the ~175 m thick and widespread sequence of Stage II erupted within a period as short as 70 kyr [see also Schnepp *et al*. (2001)], although the analytical error does not allow a better constraint on this period. Up-section in Stage II there appears to be a broad and gradual change from tholeiites to alkali basalts, suggesting that the influence of the asthenospheric source becomes gradually more important. Ar–Ar dating suggests that melting of pure asthenosphere may have lasted for a considerable period, up to 2 Myr (16·6–14·7 Ma).

SUPPLEMENTARY DATA

Supplementary data for this paper are available on *Journal of Petrology* online.

ACKNOWLEDGEMENTS

Reviews by J. Keller, J. M. Cebriá and K. Hoernle, and the thorough editorial efforts by M. Wilson greatly helped to improve this manuscript. Dr K. Ehrenberg is gratefully thanked for his assistance during sampling. K. Simon assisted with ICP-MS analysis, and B. Bock with Sr, Nd and Pb isotope analysis. G. Hartmann performed some of the Pb analyses reported in this study. S. Fillie, K. Jespersen, M. Frische and H. Mensah assisted with the sample preparation. Further assistance in the laboratories was given by N. Hildebrand, G. Mengel, L. Reese, A. Reitz, I. Reuber and E. Schiffczyk. This research was funded by the Deutsche Forschungsgemeinschaft through DFG grant Wo362/17.

REFERENCES

Allègre, W. J., Treuil, M., Minster, J.-F., Minster, B. & Albarède, F. (1977). Systematic use of trace elements in igneous processes Part I: fractional crystallization processes in volcanic suites. *Contributions to Mineralogy and Petrology* **60**, 57–75.

Babuska, V. & Plomerova, J. (1992). The lithosphere in Central Europe—seismological and petrological aspects. *Tectonophysics* **207**, 101–163.

Becker, A. (1993). An attempt to define a 'neotectonic period' for central and northern Europe. *Geologische Rundschau* **82**, 67–83.

Blundy, J. D., Robinson, J. A. C. & Wood, B. J. (1998). Heavy REE are compatible in clinopyroxene on the spinel lherzolite solidus. *Earth and Planetary Science Letters* **160**, 493–504.

Bogaard, P. J. F. (2000). Temporal evolution of the Vogelsberg volcano, central Germany. Mantle sources, melting processes and magma differentiation, reconstructed from the 'Forschungsbohrung Vogelsberg 1996'. Ph.D. thesis, Georg August Universität, Göttingen.

Bogaard, P., Jabri, L. & Wörner, G. (2001*a*). Chemical alteration of basalts from the drill core 'Forschungsbohrung Vogelsberg 1996', Germany. *Geologische Abhandlungen Hessen* **107**, 101–118.

Bogaard, P. J. F., Wörner, G. & Henjes-Kunst, F. (2001*b*). Chemical stratigraphy and origin of volcanic rocks from the drill-core 'Forschungbohrung Vogelsberg 1996', Germany. *Geologische Abhandlungen Hessen* **107**, 69–99.

Braun, T. & Berckhemer, H. (1993). Investigation of the lithosphere beneath the Vogelsberg volcanic complex with P-wave travel time residuals. *Geologische Rundschau* **82**, 20–29.

Brenan, J. M., Shaw, H. F., Ryerson, F. J. & Phinney, D. L. (1995). Experimental determination of trace-element partitioning between pargasite and a synthetic hydrous andesitic melt. *Earth and Planetary Science Letters* **135**, 1–11.

Cebriá, J.-M. & López-Ruiz, J. (1996). A refined method for trace element modelling of nonmodal batch melting processes: the Cenozoic continental volcanism of Calatrava, Spain. *Geochimica et Cosmochimica Acta* **60**, 1355–1366.

Cebriá, J. M. & Wilson, M. (1995). Cenozoic mafic magmatism in central Europe: a common European Asthenospheric Reservoir? *Terra Abstracts* **7**, 162.

Cebriá, J. M. & Wilson, M. (1996). Trace element composition of the European Asthenospheric Reservoir as inferred from partial melting modelling. *Journal of Conference Abstracts* **1**, 98.

Chauvel, C., Hofmann, A. W. & Vidal, P. (1992). HIMU–EM; the French Polynesian connection. *Earth and Planetary Science Letters* **110**, 99–119.

Chen, C. H. (1988). Estimation of the degree of partial melting by $(Na_2O + K_2O)$ and Al_2O_3/SiO_2 of basic magmas. *Chemical Geology* **71**, 355–364.

Chesley, J. T. & Ruiz, J. (1998). Crust–mantle interaction in large igneous provinces: implications from the Re–Os isotope systematics of the Columbia River flood basalts. *Earth and Planetary Science Letters* **154**, 1–11.

DePaolo, D. J. & Wasserburg, G. J. (1979). Petrogenetic mixing models and Nd–Sr isotopic patterns. *Geochimica et Cosmochimica Acta* **43**, 615–628.

Downes, H. & Leyreloup, A. (1986). Granulitic xenoliths from the French Massif Central—petrology, Sr and Nd isotope systematics and model age estimates. In: Dawson, J. B., Carswell, D. A., Hall, J. & Wedepohl, K. H. (eds) *The Nature of the Lower Continental Crust. Geological Society, London, Special Publications* **24**, 319–330.

Downes, H., Kempton, P. D., Briot, D., Harmon, R. S. & Leyreloup, A. F. (1991). Pb and O isotope systematics in granulite facies xenoliths, French Massif Central: implications for crustal processes. *Earth and Planetary Science Letters* **102**, 342–357.

Ehrenberg, K.-H. & Hickethier, H. (1978). *Erläuterungen zur Geologischen Karte Hessen Blatt nr. 5620 Ortenberg*. Hessisssches Landesamt für Bodenforschung.

Ehrenberg, K.-H. & Hickethier, H. (1985). Die Basaltbasis im Vogelsberg: Schollenbau und Hinweise zur Entwicklung der vulkanischen Abfolge. *Geologisches Jahrbuch Hessen* **113**, 97–135.

Ehrenberg, K.-H. & Hickethier, H. (1994). Tertiärer Vulkanismus der Wasserkuppenrhön und Kuppenrhön. *Jahresberichte und Mitteilungen des Oberrheinischen Geologischen Vereines* **76**, 83–146.

Ehrenberg, K.-H., Fromm, K., Grubbe, K., Harre, W., Hentschel, G., Hölting, B., Holtz, S., Kreuzer, H., Meisl, S., Nöring, F., Plaumann, S., Pucher, R., Strecker, G., Susic, M. & Zschau, H. J. (1981). Forschungsbohrungen im hohen Vogelsberg (Hessen). Bohrung 1 (Flösser-Schneise), Bohrung 2/2a (Hasselborn). *Geologische Abhandlungen Hessen* **81**, 1–166.

Ernst, T., Kohler, H., Schütz, D. & Schwab, R. (1970). The volcanism of the Vogelsberg (Hessen) in the north of the Rhinegraben Rift System. In: Illies, J.-H. & Müller, S. (eds) *Graben Problems. International Upper Mantle Project, Scientific Reports* **27**, 143–146.

Farnetani, D. G. & Richards, M. A. (1995). Thermal entrainment and melting in mantle plumes. *Earth and Planetary Science Letters* **136**, 251–267.

Fitton, J. G., Saunders, A. D., Larsen, L. M., Hardarson, B. S. & Norry, M. J. (1998). Volcanic rocks from the southeast Greenland margin at 63°N: composition, petrogenesis and mantle sources. In: Saunders, A. D., Larsen, H. C. & Wise, S. W., Jr (eds) *Proceedings of the Ocean Drilling Program, Scientific Results, 152*. College Station, TX: Ocean Drilling Program, pp. 331–350.

Foley, S. (1992). Vein-plus-wall-rock melting mechanisms in the lithosphere and the origin of potassic alkaline magmas. *Lithos* **28**, 435–453.

Foley, S. F., Musselwhite, D. S. & van der Laan, S. R. (1999). Melt compositions from ultramafic vein assemblages in the lithospheric mantle: a comparison of cratonic and non-cratonic settings. In: Gurney, J. J., Gurney, J. L., Pascoe, M. D. & Richardson, S. H. (eds) *Proceedings of the 7th International Kimberlite Conference*. Cape Town: Red Roof Design, pp. 238–246.

Frey, F. A. (1984). Rare earth element abundances in upper mantle rocks. In: Henderson, P. (ed.) *Rare Earth Element Geochemistry. Developments in Geochemistry* **2**, 153–203.

Gallagher, K. & Hawkesworth, C. (1992). Dehydration melting and the generation of continental flood basalts. *Nature* **358**, 57–59.

Goes, S., Spakman, W. & Bijwaard, H. (1999). A lower mantle source for Central European volcanism. *Science* **286**, 1928–1931.

Granet, M., Wilson, M. & Achauer, U. (1995). Imaging a mantle plume beneath the French Massif Central. *Earth and Planetary Science Letters* **136**, 281–296.

Hall, G. E. M. & Plant, J. A. (1992). Analytical errors in the determination of high field strength elements and their implications in tectonic interpretation studies. *Chemical Geology* **95**, 141–156.

Hart, S. R. (1984). A large-scale isotope anomaly in the Southern Hemisphere mantle. *Nature* **309**, 753–757.

Hartmann, G. & Wedepohl, K. H. (1990). Metasomatically altered peridotite xenoliths from the Hessian Depression (Northwest Germany). *Geochimica et Cosmochimica Acta* **54**, 71–86.

Hawkesworth, C. J. & Gallagher, K. (1993). Mantle hotspots, plumes and regional tectonics as causes of intraplate magmatism. *Terra Nova* **5**, 552–559.

Hawkesworth, C. J., Rogers, N. W., van Calsteren, P. W. C. & Menzies, M. A. (1984). Mantle enrichment processes. *Nature* **311**, 331–333.

Hoernle, K., Zhang, Y. S. & Graham, D. (1995). Seismic and geochemical evidence for large-scale mantle upwelling beneath the eastern Atlantic and western and central Europe. *Nature* **374**, 34–39.

Hofmann, A. W. & Feigenson, M. D. (1983). Case studies on the origin of basalt I: Theory and reassessment of Grenada basalts. *Contributions to Mineralogy and Petrology* **84**, 382–389.

Ionov, D. A. & Hofmann, A. W. (1995). Nb–Ta-rich mantle amphiboles and micas: implications for subduction-related trace element fractionations. *Earth and Planetary Science Letters* **131**, 341–356.

Johnson, K. T. M., Dick, H. J. B. & Shimizu, N. (1990). Melting in the oceanic upper mantle: an ion microprobe study of diopsides in abyssal peridotites. *Journal of Geophysical Research* **95**, 2661–2678.

Jung, S. & Hoernes, S. (2000). The major- and trace-element and isotope (Sr, Nd, O) geochemistry of Cenozoic alkaline rift-type volcanic rocks from the Rhön area (central Germany): petrology, mantle source characteristics and implications for asthenosphere–lithosphere interactions. *Journal of Volcanology and Geothermal Research* **99**, 27–53.

Jung, S. & Masberg, P. (1998). Major- and trace-element systematics and isotope geochemistry of Cenozoic mafic volcanic rocks from the Vogelsberg (central Germany); constraints on the origin of continental alkaline and tholeiitic basalts and their mantle sources. *Journal of Volcanology and Geothermal Research* **86**, 151–177.

Kempton, P. D., Harmon, R. S., Stosch, H. G., Hoefs, J. & Hawkesworth, C. J. (1988). Open-system O-isotope behaviour and trace element enrichment in the sub-Eifel mantle. *Earth and Planetary Science Letters* **89**, 273–287.

Klein, E. M. & Langmuir, C. H. (1989). Local versus global variations in ocean ridge basalt composition: a reply. *Journal of Geophysical Research* **94**, 4241–4252.

Kreuzer, H., Kunz, K., Müller, P., Schenk, E., Harre, W. & Raschka, H. (1974). Petrologie und Kalium/Argon-Daten einiger Basalte aus der Bohrung 31, Rainrod I (Vogelsberg). *Geologisches Jahrbuch* **D9**, 67–84.

LaTourette, T., Hervig, R. L. & Holloway, J. R. (1995). Trace element partitioning between amphibole, phlogopite, and basanite melt. *Earth and Planetary Science Letters* **135**, 13–30.

Loock, G., Stosch, H.-G. & Seck, H. A. (1990). Granulite facies lower crustal xenoliths from the Eifel, West Germany: petrological and geochemical aspects. *Contributions to Mineralogy and Petrology* **105**, 25–41.

MacDonald, G. A. (1968). Composition and origin of Hawaiian lavas. In: Coats, R. R., Hay, R. L. & Anderson, C. A. (eds) *Studies in Volcanology: a Memoir in Honour of Howel Williams*. Boulder, CO: Geological Society of America, pp. 477–522.

McDonough, W. F. & Frey, F. A. (1989). Rare earth elements in upper mantle rocks. In: Lipin, B. R. & McKay, G. A. (eds) *Geochemistry and Mineralogy of Rare Earth Elements. Mineralogical Society of America, Reviews in Mineralogy* **21**, 100–145.

McKenzie, D. & Bickle, M. J. (1988). The volume and composition of melt generated by extension of the lithosphere. *Journal of Petrology* **29**, 625–679.

McKenzie, D. & O'Nions, R. K. (1991). Partial melt distributions from inversion of rare earth element concentrations. *Journal of Petrology* **32**, 1021–1091.

Mengel, K., Sachs, P. M., Stosch, H. G., Wörner, G. & Loock, G. (1991). Crustal xenoliths from Cenozoic volcanic fields of West Germany: implications for structure and composition of the continental crust. *Tectonophysics* **195**, 271–289.

Merle, O., Michon, L., Camus, G. & de Goer, A. (1998). L'extension oligocène sur la transversale septentrionale de rift du Massif central. *Bulletin de la Societe Géologique de France* **169**, 615–626.

Minster, J. F. & Allègre, C. J. (1978). Systematic use of trace elements in igneous processes Part III: inverse problem of batch partial melting in volcanic suites. *Contributions to Mineralogy and Petrology* **68**, 37–52.

Muenker, C. (1998). Nb/Ta fractionation in a Cambrian arc/back arc system, New Zealand; source constraints and application of refined ICPMS techniques. *Chemical Geology* **144**, 23–45.

O'Reilly, S. Y. & Zhang, M. (1995). Geochemical characteristics of lava-field basalts from eastern Australia and inferred sources: connections with the subcontinental lithospheric mantle? *Contributions to Mineralogy and Petrology* **121**, 148–170.

Ormerod, D. S., Hawkesworth, C. J., Rogers, N. W., Leeman, W. P. & Menzies, M. A. (1988). Tectonic and magmatic transitions in the Western Great Basin, USA. *Nature* **333**, 349–353.

Raikes, S. & Bonjer, K.-P. (1983). Large-scale mantle heterogeneity beneath the Rhenish Massif and its vicinity from teleseismic P-residuals measurements. In: Fuchs, K., von Gehlen, K., Mälzer, H., Murawski, H. & Semmel, A. (eds) *Plateau Uplift*. Berlin: Springer, pp. 315–331.

Ritter, J. R. R., Jordan, M., Christensen, U. R. & Achauer, U. (2001). A mantle plume below the Eifel volcanic fields, Germany. *Earth and Planetary Science Letters* **186**, 7–14.

Rosenbaum, J. M. & Wilson, M. (1996). Two-stage enrichment of the Eifel mantle: new evidence. *Journal of Conference Abstracts* **1**, 523.

Rudnick, R. L. & Goldstein, S. L. (1990). The Pb isotopic compositions of lower crustal xenoliths and the evolution of lower crustal Pb. *Earth and Planetary Science Letters* **98**, 192–207.

Sachs, P. M. & Hansteen, T. H. (2000). Pleistocene underplating and metasomatism of the lower continental crust: a xenolith study. *Journal of Petrology* **41**, 331–356.

Schnepp, E., Rolf, C. & Struck, J. (2001). Paläo- un gesteinsmagnetische Untersuchungen an Kernen der Forschungsbohrung Vogelsberg 1996. *Geologische Abhandlungen Hessen* **107**, 151–169.

Schreiber, U. & Rotsch, S. (1998). Cenozoic block rotation according to a conjugate shear system in central Europe—indications from paleomagnetic measurements. *Tectonophysics* **299**, 111–142.

Spera, F. J. & Bohrson, W. A. (2001). Energy-constrained open-system magmatic processes I: general model and energy-constrained assimilation and fractional crystallization (EC-AFC) formulation. *Journal of Petrology* **42**, 999–1018.

Stosch, H.-G. & Lugmair, G. W. (1984). Evolution of the lower continental crust: granulite facies xenoliths from the Eifel, West Germany. *Nature* **311**, 368–370.

Stosch, H.-G. & Lugmair, G. W. (1986). Trace element and Sr and Nd isotope geochemistry of peridotite xenoliths from the Eifel (West Germany) and their bearing on the evolution of the subcontinental lithosphere. *Earth and Planetary Science Letters* **80**, 281–298.

Stosch, H. G. & Seck, H. A. (1980). Geochemistry and mineralogy of two spinel peridotite suites from Dreiser Weiher, West Germany. *Geochimica et Cosmochimica Acta* **44**, 457–470.

Stosch, H.-G., Lugmair, G. W. & Seck, H. A. (1986). Geochemistry of granulite-facies lower crustal xenoliths: implications for the geological history of the lower continental crust below the Eifel, West Germany. In: Dawson, J. B., Carswell, D. A., Hall, J. & Wedepohl, K. H. (eds) *The Nature of the Lower Continental Crust. Geological Society, London, Special Publications* **24**, 309–317.

Sun, S.-S. & McDonough, W. F. (1989). Chemical and isotopic systematics of oceanic basalts: implications for mantle composition and processes. In: Saunders, A. D. & Norry, M. J. (eds) *Magmatism in the Ocean Basins. Geological Society, London, Special Publications* **42**, 313–345.

Thirlwall, M. F. & Jones, N. W. (1983). Isotope geochemistry and contamination mechanisms of Tertiary lavas from Skye, northwest Scotland. In: Hawkesworth, C. J. & Norry, M. J. (eds) *Continental Basalts and Mantle Xenoliths*. Nantwich: Shiva, pp. 186–208.

Thirlwall, M. F., Upton, B. G. J. & Jenkins, C. (1994). Interaction between continental lithosphere and the Iceland plume—Sr–Nd–Pb isotope geochemistry of Tertiary basalts, NE Greenland. *Journal of Petrology* **35**, 839–879.

Totland, M., Jarvis, I. & Jarvis, K. E. (1992). An assessment of dissolution techniques for the analysis of geological samples by plasma spectrometry. *Chemical Geology* **95**, 35–62.

Villemant, B., Jaffrezic, H., Joron, J.-L. & Treuil, M. (1981). Distribution coefficients of major and trace elements; fractional crystallization in the alkali basalt series of Chaîne des Puys (Massif Central, France). *Geochimica et Cosmochimica Acta* **45**, 1997–2016.

Wedepohl, K. H. (1985). Origin of the Tertiary basaltic volcanism in the Hessian Depression. *Contributions to Mineralogy and Petrology* **89**, 122–143.

Wedepohl, K. H. & Baumann, A. (1999). Central European Cenozoic plume volcanism with OIB characteristics and indications of a lower mantle source. *Contributions to Mineralogy and Petrology* **136**, 225–239.

Wedepohl, K. H., Gohn, E. & Hartmann, G. (1994). Cenozoic alkali basaltic magmas of western Germany and their products of differentiation. *Contributions to Mineralogy and Petrology* **115**, 253–278.

White, R. & McKenzie, D. (1989). Magmatism at rift zones: the generation of volcanic continental margins and flood basalts. *Journal of Geophysical Research* **94**, 7685–7729.

Wilson, M. & Downes, H. (1991). Tertiary–Quaternary extension-related alkaline magmatism in Western and Central Europe. *Journal of Petrology* **32**, 811–849.

Wilson, M. & Patterson, R. (2002). Intraplate magmatism related to short-wavelength convective instabilities in the upper mantle: evidence from the Tertiary–Quaternary volcanic province of western and central Europe. *Geological Society of America, Special Papers* **352**, 37–58.

Witt-Eickschen, G. (1993). Upper mantle xenoliths from alkali basalts of the Vogelsberg, Germany: implications for mantle upwelling and metasomatism. *European Journal of Mineralogy* **5**, 361–376.

Witt-Eickschen, G. & Kramm, U. (1997). Mantle upwelling and metasomatism beneath Central Europe: geochemical and isotopic constraints from mantle xenoliths from the Rhön (Germany). *Journal of Petrology* **38**, 479–493.

Witt-Eickschen, G. & Kramm, U. (1998). Evidence for the multiple stage evolution of the subcontinental lithospheric mantle beneath the Eifel (Germany) from pyroxenite and composite pyroxenite/peridotite xenoliths. *Contributions to Mineralogy and Petrology* **131**, 258–272.

Witt-Eickschen, G., Kaminsky, W., Kramm, U. & Harte, B. (1998). The nature of young vein metasomatism in the lithosphere of the West Eifel (Germany): geochemical and isotopic constraints from composite mantle xenoliths from the Meerfelder Maar. *Journal of Petrology* **39**, 155–185.

Wittenbecher, M. (1992). Geochemie tholeiitischer und alkali-olivinbasaltischer Gesteine des Vogelsberges. *Geologische Abhandlungen Hessen* **97**, 3–52.

Wörner, G., Zindler, A., Staudigel, H. & Schmincke, H. U. (1986). Sr, Nd and Pb geochemistry of Tertiary and Quaternary alkaline volcanics from West Germany. *Earth and Planetary Science Letters* **79**, 107–119.

Zack, T., Foley, S. F. & Jenner, G. A. (1997). A consistent partition coefficient set for clinopyroxene, amphibole and garnet from laser ablation microprobe analysis of garnet pyroxenites from Kakanui, New Zealand. *Neues Jahrbuch für Mineralogie, Abhandlungen* **172**, 23–41.

Zindler, A. & Hart, S. (1986). Chemical geodynamics. *Annual Review of Earth and Planetary Sciences* **14**, 493–571.